JCI The Journal of Clinical Investigation

Androgen aggravates aortic aneurysms via suppressing PD-1 in mice

Xufang Mu, … , Ming C. Gong, Zhenheng Guo

J Clin Invest. 2024. https://doi.org/10.1172/JCI169085.

Research In-Press Preview Inflammation Vascular biology

Graphical abstract

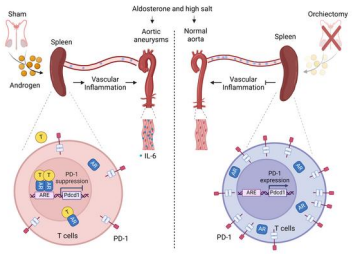

Androgen aggravates aortic aneurysms via suppressing PD-1 in mice

Xufang Mu[1,], Shu Liu[2,], Zhuoran Wang[1], Kai Jiang[2], Tim McClintock[2], Arnold J. Stromberg[3,†], Alejandro V.Tezanos[3], Eugene S Lee[4], John A. Curci[5], Ming C Gong[2,6,*], and Zhenheng Guo[1,6,7,*]

[1]Departments of Pharmacology and Nutritional Sciences, [2]Physiology, [3]Statistics, and [6]Saha Cardiovascular Research Center, University of Kentucky, Lexington, KY; [4]Department of Research, Sacramento VA Medical Center, Mather, CA; [5]Department of Vascular Surgery, Vanderbilt University, Nashville, TN; [7]Department of Research, Lexington Veterans Affairs Medical Center, Lexington, KY, USA

The authors have declared that no conflict of interest exists

[†]Deceased September 17, 2023

[*]To whom correspondence should be addressed:

Ming C. Gong, Ph.D.
509 Wethington Building
900 South Limestone Street
Lexington, KY 40536
Phone: (859)218-1361
Email: ming.gong@uky.edu

Zhenheng Guo, Ph.D.
515 Wethington Building
900 South Limestone Street
Lexington, KY 40536
Phone: (859)218-1416
email: zguo2@uky.edu

Abstract

Androgen has long been recognized for its pivotal role in the sexual dimorphism of cardiovascular diseases, including aortic aneurysms, a devastating vascular disease with a higher prevalence and fatality rate in men than women. However, the mechanism by which androgen mediates aortic aneurysms is largely unknown. Herein, we found that male mice, not female mice, developed aortic aneurysms when exposed to aldosterone and high salt (Aldo-salt). We revealed that androgen and androgen receptors (AR) were crucial for this sexually dimorphic response to Aldo-salt. We identified programmed cell death protein 1 (PD-1), an immune checkpoint, as a key link between androgen and aortic aneurysms. We demonstrated that administration of anti-PD-1 Ab and adoptive PD-1 deficient T cell transfer reinstated Aldo-salt-induced aortic aneurysms in orchiectomized mice, and genetic deletion of PD-1 exacerbated aortic aneurysms induced by high-fat diet and angiotensin II (Ang II) in non-orchiectomized mice. Mechanistically, we discovered that AR bound to the PD-1 promoter to suppress its expression in the spleen. Thus, our study unveils a mechanism by which androgen aggravates aortic aneurysms by suppressing PD-1 expression in T cells. Moreover, our study suggests that some cancer patients might benefit from screenings for aortic aneurysms during immune checkpoint therapy.

Graphical Abstract

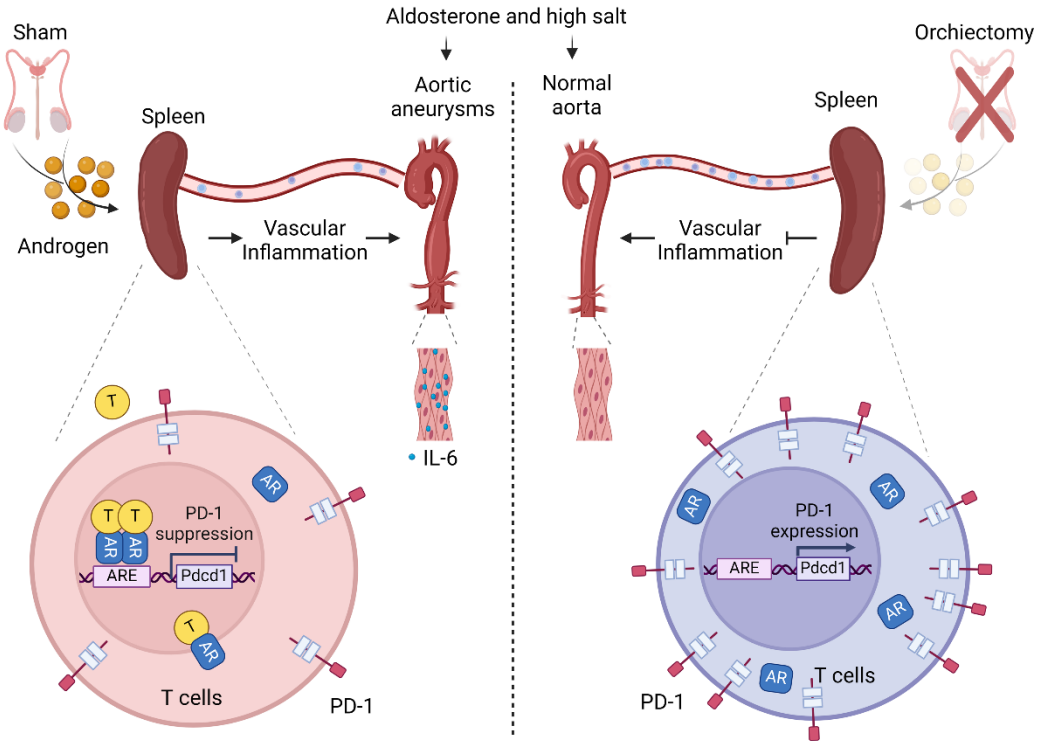

Introduction

Aortic aneurysms are defined as a permanent localized dilation of the aorta and can be classified as thoracic aortic aneurysms (TAA) and abdominal aortic aneurysms (AAA) (1). Aortic aneurysms are usually asymptomatic until they rupture, often lethal, resulting in over 85% mortality (2). Currently, no medication except for surgery is approved to treat this devastating vascular disease.

Epidemiologic studies reveal aging, male sex, smoking, atherosclerosis, and hypertension as the risk factors for aortic aneurysms (3). In particular, the male sex is considered the most potent nonmodified risk factor for the sexual dimorphism of aortic aneurysms, with a 4:1 male-to-female ratio (3). While the etiology of the sex difference in human aortic aneurysms remains to be elucidated, accumulated evidence from animal studies demonstrated that both sex chromosomes and hormones contributed to the development of aortic aneurysms (4). In particular, it is well documented that gonadal androgen but not estrogen deprivation protects angiotensin II (Ang II)- or elastase-induce aortic aneurysms (5-7), indicating that androgen likely plays a predominant role in the sexual dimorphism of aortic aneurysms. However, the mechanism by which androgen aggravates Ang II or elastin-induced aortic aneurysms remains largely unknown.

Accumulated clinical evidence demonstrates that elevated plasma concentration of Aldo, an essential component of the renin-angiotensin-aldosterone system, and excessive dietary sodium intake are associated with an increased risk for hypertension, stroke, coronary heart disease, heart failure, and renal disease (8). Consistent with these human studies, we developed a mouse model of aortic aneurysms in which we administered Aldo and high salt (Aldo-salt) to 10-month-old male C57BL/6J mice (9, 10). Importantly, we demonstrated that Aldo-salt-induced aortic aneurysms depend on age and mineralocorticoid receptor (MR; also known as Aldo receptor) but not Ang II receptor (9, 10). However, whether Aldo-salt-induced aortic aneurysms have a sexual dimorphism has not been investigated.

In this study, we report that Aldo-salt-induced aortic aneurysms mimicked human aortic aneurysms, exhibiting a strong sexual dimorphism. To delve into the role of androgen in this sexual dimorphism, we conducted a series of animal experiments, including gonadal androgen deprivation via orchiectomy, restoration of androgen in orchiectomized mice through dihydrotestosterone (DHT) pellet implantation, and downregulation of androgen receptors (AR) by ASC-J9 or inhibition of AR by flutamide. Our results consistently underscore the critical involvement of androgen and AR in Aldo-salt-induced aortic aneurysms. To investigate the mechanism by which androgen mediates Aldo-salt-induced aortic aneurysms, we found that Aldo-salt-induced IL-6 expression was selectively abolished in the aorta by orchiectomy. Subsequent inhibition of IL-6 signaling by LMT-28 illustrated that IL-6 is implicated in Aldo-salt-induced aortic aneurysms. Moreover, through RNA-seq and flow cytometry analysis of the aortas, we identified T cell receptor (TCR) and PD-1, an immune checkpoint (11), as a pivotal link between androgen and Aldo-salt-induced aortic aneurysms. Splenectomy augmented PD-1^+ T and B cells in the aorta and mitigated Aldo-salt-induced aortic aneurysms. Mechanistically, we discovered that AR bound to the PD-1 promoter and suppressed its mRNA and protein expression in the spleen in mice administered Aldo-salt. To define the role of PD-1 in the pathogenesis of aortic aneurysms, we demonstrated that immune checkpoint blockade with anti-PD-1 Ab and adoptive PD-1 deficient T cell transfer restored Aldo-salt-induced aortopathies in orchiectomized mice. Finally, we showed that genetic deletion of PD-1 exacerbated HFD and Ang II-induced aortopathy in non-orchiectomized mice. Collectively, our results provide mechanistic insight into the role of androgen in the pathogenesis of aortic aneurysms and suggest a potential risk of aortic aneurysm development in cancer patients undergoing immune checkpoint therapy.

Results

Sexual dimorphism in Aldo-salt-induced aortic aneurysms

To investigate sexual dimorphism in Aldo-salt-induced aortic aneurysms, 10-month-old male and female C57BL/6J mice were subjected to Aldo-salt administration for four weeks to induce aortic aneurysms (9, 10). Suprarenal aortic dilations induced by Aldo-salt were monitored weekly by ultrasound (9, 10). Albeit Aldo-salt induced suprarenal aortic dilation in both male and female mice in a time-dependent manner, the suprarenal aortic dilation induced by Aldo-salt was much larger in male than in female mice (Figure 1A). Utilizing the ultrasound data, we calculated the growth rate of the suprarenal aortic diameters, an important clinical index for appraisal of aortic aneurysm progression and rupture in human patients (4). Consistently, the suprarenal aortic growth rate was significantly accelerated in male than female mice (Figure 1B).

To define the role of hypertension in the sexual dimorphism of Aldo-salt-induced aortic aneurysms, we assessed mean arterial pressure (MAP) in the male and female mice by tail cuff one week before and three weeks after Aldo-salt administration. Both male and female mice displayed a hypertensive response to Aldo-salt. Surprisingly, female mice exhibited higher MAP levels than male mice before and after Aldo-salt administration (Figure 1C), suggesting that the greater increase in the suprarenal aortic dilation induced by Aldo-salt is not attributed to hypertension.

Four weeks after Aldo-salt administration, the aortas were harvested from the male and female mice for morphometric analysis. Maximal external diameters of the ascending aorta (AscAo), aortic arch (ArchAo), descending aorta (DesAo), and suprarenal aorta (SupAo) were measured (Supplemental Figure 1). While no differences were observed in the baseline, a significant increase in the external diameters of the AscAo, DesAo, and SupAo was noted in response to Aldo-salt in male mice compared to female mice (Figures 1D−1G). Isolated aortas were also subjected to pathological analysis to assess the incidence of the total aortic aneurysms (total AA = AAA + TAA + aortic

rupture), AAA, TAA, and aortic rupture (Figure 1H) (9, 10, 12). Remarkably, none of the female mice developed aortic aneurysms, whereas 70% of male mice exhibited aortic aneurysms, with 60% AAA, 40% TAA, and 10% aortic rupture (Figure 1I).

Gonadal androgen deprivation protects mice from Aldo-salt-induced aortic aneurysms

To explore the role of androgen in the sexual dimorphism in Aldo-salt-induced aortic aneurysms, 10-month-old male C57BL/6J mice underwent either orchiectomy or sham operation, and two weeks later, they were administered Aldo-salt for four weeks. The ratio of seminal vesicle weight (SVW) to BW was evaluated four weeks after Aldo-salt administration to confirm the success of orchiectomy. Significantly reduced SVW/BW ratios were observed in orchiectomized mice compared to sham-operated counterparts (Figure 2A and Supplemental Figures 2A and 2B). Additionally, serum testosterone levels were significantly lower in orchiectomized mice compared to sham-operated mice (Supplemental Figure 2C). Importantly, compared to the sham operation, orchiectomy markedly suppressed Aldo-salt-induced suprarenal aortic dilation and progression (Figures 2B and 2C), the external diameters of the aorta, including the AscAo, ArchAo, DesAo, and SupAo (Figure 2D), and the incidence of AAA and TAA (Figure 2E).

The severity of Aldo-salt-induced aortic aneurysms resembles human aortic aneurysms (13) and exhibits significant variability (9, 10). Similar to Ang II-induced aortic aneurysms (12), the severity of Aldo-salt-induced aortic aneurysms could be categorized into Type I, II, III, and IV (Supplemental Figure 3). Compared to sham operation, orchiectomy reduced the percentage of Type II and III but not Type I aortic aneurysms (Figures 2F and 2G), indicating that androgen may mainly affect the progression of Aldo-salt-induced aortic aneurysms.

To investigate whether androgen augments Aldo-salt-induced aortic aneurysms through salt retention, we assessed 24-h sodium retention in orchiectomized and sham-operated mice by

subtracting their 24-h sodium excretion (via urine) from their sodium intake (via food and water intake) (14) one week before and three weeks after Aldo-salt administration. Interestingly, orchiectomy increased both 24-h sodium intake and 24-urinary sodium excretion compared to the sham operation (Supplemental Figures 4A−4E). As a net balance, orchiectomy did not significantly alter Aldo-salt-induced sodium retention (Supplemental Figure 4F). Consistent with these findings, there was no significant difference in serum sodium levels between the orchiectomized and sham-operated mice, and no correlation was observed between the serum sodium level and the internal diameter of the suprarenal aorta four weeks after Aldo-salt administration (Supplemental Figures 4G and 4H). Additionally, serum sodium levels did not differ between the orchiectomized and sham-operated mice, regardless of whether the mice developed aortic aneurysms (Supplemental Figure 4I).

To investigate whether androgen augments Aldo-salt-induced aortic aneurysms through hypertension, we evaluated the effect of orchiectomy on MAP by tail-cuff measurement one week before and three weeks after Aldo-salt administration. In line with its minimal effect on sodium retention, orchiectomy did not affect MAP before and after Aldo-salt administration (Supplemental Figure 4J). Moreover, no correlation was observed between MAP and the internal diameter of the suprarenal aorta three weeks after Aldo-salt administration (Supplemental Figure 4K), and no significant disparities in MAP were noted between orchiectomized and sham-operated mice, regardless of whether the development of aortic aneurysms (Supplemental Figure 4L). Similar findings were also observed in systolic and diastolic blood pressure (Gong and Guo, unpublished observation).

Restoration of androgen in orchiectomized mice reinstates Aldo-salt-induced aortic aneurysms

To further elucidate the role of androgen in Aldo-salt-induced aortic aneurysms, 10-month-old male C57BL/6J mice underwent orchiectomy, and two weeks later, they were administered Aldo-salt with

or without dihydrotestosterone (DHT) pellet implantation (10 mg, 60-day release (6)) for four weeks. DHT was chosen over testosterone due to its greater potency and inability to be converted to estrogens by aromatase (15), ensuring a more straightforward interpretation of results. DHT effectively restored the SVW/BW ratio in orchiectomized mice to levels comparable to those in sham-operated mice DHT four weeks after Aldo-salt administration (Figure 3A and Supplemental Figures 2A, 2B, and 5), indicating the functionality of the implanted DHT pellets in mice. Importantly, compared to orchiectomized mice without DHT, those with DHT exhibited a trend or significant increase in response to Aldo-salt in the internal diameters and growth rate of SupAo (Figures 3B and 3C), the external diameters of the AscAo, ArchAo, DesAo, and SupAo (Figure 3D), and the incidence of aortic aneurysms, including AAA, TAA, and aortic rupture (Figure 3E).

The aortopathy in orchiectomized mice administered Aldo-salt with DHT appeared more pronounced than in sham-operated mice (Figures 3F and 3G *vs.* 2F and 2G). To quantitatively assess the extent to which DHT restores Aldo-salt-induced aortic aneurysms, we calculated the percentage of aortic aneurysm restoration rates by normalizing the incidence of aortic aneurysms in orchiectomized mice with DHT (Figure 3E) to that in sham-operated mice (Figure 2E). As a result, 80%, 83%, and 73% of aortic aneurysm restoration rates were obtained in orchiectomized mice administered Aldo-salt with DHT for total AA, AAA, and TAA, respectively (Figure 3H).

Surprisingly, DHT significantly suppressed 24-h sodium intake and 24-h urinary sodium excretion three weeks after Aldo-salt administration (Supplemental Figures 6A−6E). However, DHT did not significantly affect Aldo-salt-induced sodium retention, serum sodium levels, and hypertension (Supplemental Figures 6F, 6G, and 6J). There was no significant correlation between the internal diameter of the suprarenal aorta and serum sodium or MAP levels in orchiectomized mice administered Aldo-salt with and without DHT (Supplemental Figures 6H and 6K). Furthermore, there was no significant difference in serum sodium or MAP levels in orchiectomized mice administered

Aldo-salt with or without DHT, regardless of whether they developed aortic aneurysms (Supplemental Figures 6I and 6L). Thus, DHT is unlikely to restore Aldo-salt-induced aortic aneurysms through sodium retention and hypertension.

Downregulation of AR ameliorates Aldo-salt-induced aortic aneurysms

To explore targeting androgen as a potential therapy for treating aortic aneurysm, 10-month-old male C57BL/6J mice were administered Aldo-salt with or without ASC-J9 (50 mg/kg, i.p. injection, once a day) for four weeks (16). ASC-J9, a recently developed AR-degradation enhancer, has been shown to selectively degrade AR without affecting other nuclear receptors (17). The efficacy of ASC-J9 in promoting AR protein degradation was confirmed via IHC in the suprarenal aorta of mice four weeks after Aldo-salt administration, with or without ASC-J9 (Figure 4A). Importantly, similar to the effect of orchiectomy (Figure 2), ASC-J9 effectively mitigated Aldo-salt-induced suprarenal aortic dilation and progression (Figures 4B and 4C), the external diameters of the AscAo and SupAo (Figure 4D), and the incidence and severity of aortic aneurysms (Figures 4E−4G).

Intriguingly, ASC-J9 suppressed Aldo-salt-induced 24-h sodium intake and urinary sodium excretion (Supplemental Figures 7A−7E). However, similar to the effect of orchiectomy and DHT (Supplemental Figures 4 and 6), ASC-J9 also did not affect Aldo-salt-induced sodium retention, hypernatremia, and hypertension (Supplemental Figures 7F, 7G, and 7J). There was no significant correlation between the internal diameters of the suprarenal aorta and serum sodium or MAP in mice administered Aldo-salt with and without ASC-J9 (Supplemental Figures 7H and 7K). Furthermore, there was no significant difference in serum sodium or MAP levels between mice with and without ASC-J9, regardless of whether they developed aortic aneurysms (Supplemental Figures 7I and 7L). Thus, ASC-J9 is unlikely to protect mice from Aldo-salt-induced aortic aneurysms through sodium retention and hypertension.

ASC-J9 was reported to exert its effects through AR-dependent and independent mechanisms (18). To verify whether ASC-J9 protects mice from Aldo-salt-induced aortic aneurysms via AR, 9-10-month-old male C57BL/6J mice were administered Aldo-salt with flutamide (50 mg/kg/day, i.p. injection, once a day) or vehicle for four weeks (19). Flutamide, a selective AR antagonist, has been clinically utilized to treat patients with prostate cancer (19). In line with the effects of ASC-J9 (Figure 4), flutamide reduced the seminal vesicle weight (Supplemental Figure 8A−8C) and, more importantly, protected mice from Aldo-salt-induced suprarenal aortic dilation and progression and the incidence of AAA (Supplemental Figures 8D−8G). Interestingly, flutamide did not affect basal MAP but moderately boosted Aldo-salt-induced hypertension (Supplemental Figure 8H).

IL-6 is implicated in Aldo-salt-induced and androgen-mediated aortic aneurysms

To investigate the molecular mechanism by which androgen mediates Aldo-salt-induced aortic aneurysms, we conducted real-time PCR to analyze mRNA expressions in the aortas from 10-month-old orchiectomized and sham-operated C57BL/6J mice, with and without Aldo-salt administration for ten days. We opted to isolate the aortas ten days rather than four weeks after Aldo-salt administration because we sought to identify androgen-targeting genes that result in rather than result from Aldo-salt-induced aortic aneurysms.

Based on the literature (9, 10, 16, 20-22), we focused on a list of genes implicated in aortic aneurysms, including *Ar*, *Nr3c2*, *Sgk1*, *Scnn1a*, *Scnn1b*, *Scnn1g*, *Bmal1*, *Tgfb2*, *Mmp2*, *Il1b*, *Il6*, *Il6ra*, *Il6st*, *Ccl2*, *Ccl4*, and *Tnf*. Of the 16 genes examined, 12 genes (*Ar, Nr3C2, Sgk1, Scnn1a, Scnn1b, Scnn1g, Bmal1, Il1b, Il6, Il6ra, Ccl2,* and *Ccl4*) responded to Aldo-salt: 9 of them (*Ar, Nr3C2, Sgk1, Scnn1a, Scnn1b, Scnn1g, Il1b, Il6ra,* and *Ccl4*) were downregulated, whereas 3 of them (*Bmal1, Il6,* and *Ccl2*) were upregulated (Supplemental Figure 9). Interestingly, 5 genes (*Nr3C2, Scnn1a, Scnn1b, Il6,* and *Ccl2*) also responded to orchiectomy after Aldo-salt administration: 3 of them (*Nr3C2, Scnn1a, Scnn1b*) were upregulated, whereas 2 of them, (*Il6,* and *Ccl2*) were downregulated

(Supplemental Figures 9B, 9D, 9E, 9K, and 9N). Particularly noteworthy, *Il6* was found to be most dramatically upregulated by Aldo-salt (i.e., up to 58-fold), which was completely abolished by orchiectomy (Supplemental Figure 9K).

IL-6 is implicated in human aortic aneurysms (22). Therefore, we focused on IL-6 and further investigated whether its protein expression is regulated by Aldo-salt and/or androgen in the suprarenal aorta of 10-month-old orchiectomized and sham-operated C57BL/6J mice with and without 10-day Aldo-salt administration. In sham-operated mice, basal IL-6 protein expression was barely detectable in the suprarenal aorta, whereas IL-6 protein was markedly upregulated by Aldo-salt in the suprarenal aorta. Intriguingly, orchiectomy increased basal IL-6 protein expression but decreased Aldo-salt-induced IL-6 protein upregulation in the suprarenal aorta (Supplemental Figures 10A and 10B). In contrast to IL-6 protein, MR protein did not respond to Aldo-salt and/or orchiectomy in the suprarenal aorta (Supplemental Figures 10C and 10D).

While the elevated basal IL-6 protein expression in the suprarenal aorta induced by orchiectomy may be attributed to the loss of androgen-induced immunosuppression (20), the abrogation of Aldo-salt-induced IL-6 protein upregulation elicited by orchiectomy might be due to a blockade of Aldo-salt-induced inflammatory cell infiltration in the aorta (9, 10), specifically macrophages, which are known for their pivotal role in IL-6 production (8). To explore this possibility, we investigated whether orchiectomy affects Aldo-salt-induced macrophage infiltration by IHC in the suprarenal aorta of 10-month-old male C57BL/6J mice with and without 10-day Aldo-salt administration. Interestingly, orchiectomy abolished Aldo-salt-induced immunostaining of F4/80, a macrophage marker, in the suprarenal aortas (Supplemental Figures 11A and 11B).

To investigate the potential role of IL-6 in Aldo-salt-induced aortic aneurysms, 10-month-old male C57BL/6J mice were administered Aldo-salt with LMT-28 (0.25 mg/kg, oral gavage, once a day) or

vehicle for four weeks (23). LMT-28, a recently developed novel small molecule inhibitor, has been shown to specifically target IL-6Rβ to disrupt its interaction with IL-6Rα, thus inhibiting IL-6 signaling (23). The efficacy of LMT-28 in inhibiting IL-6 signaling was confirmed by immunostaining of phosphorylated STAT3, an index of the IL-6 signaling activation (23), in the suprarenal aortas by IHC in the mice four weeks after Aldo-salt with LMT-28 or vehicle administration (Figure 5A). Importantly, compared to vehicles, LMT-28 protected mice from Aldo-salt-induced suprarenal aortic dilation and progression (Figures 5B−5C), as well as the incidence and severity of aortic aneurysms (Figures 5E−5G). It is noteworthy, however, that LMT-28 did not affect the external diameters of the aorta (Figure 5D).

Interestingly, LMT-28 increased Aldo-salt-induced salt retention but did not affect serum sodium and MAP levels before and after Aldo-salt administration (Supplemental Figures 12A−12D and 12G). Notably, there was no significant correlation between the internal diameter and serum sodium or MAP levels (Supplemental Figures 12E and 12H). Additionally, there was no significant difference in serum sodium level and MAP levels between mice with and without LMT-28, irrespective of whether they developed aortic aneurysms (Supplemental Figures 12F and 12I).

Aldo-salt may induce aortic aneurysms through AR and androgen synthesis pathways. To explore this possibility, we determined AR protein expression by IHC and androgen synthesis (*Cyp17a1*, *Hsd3b2*, and *Hsd17b3*) (24)) mRNA expressions by real-time PCR in the aorta, testis, and adrenal gland from 10-month-old male C57BL/6J mice ten days after Aldo-salt administration. The results revealed that Aldo-salt neither affected AR protein expression in the suprarenal aortas (Supplemental Figures 13A and 13B) nor *Cyp17a1*, *Hsd3b2*, and *Hsd17b3* mRNA expressions in the testis (Supplemental Figures 13C−13E). Interestingly, Aldo-salt moderately inhibited *Cyp17a1* and *Hsd17b3* but not *Hsd3b2* mRNA expressions in the adrenal gland (Supplemental Figures 13F−13H). However, there was no significant difference in plasma testosterone levels between mice with and without Aldo-

salt administration (Supplemental Figure 13I).

Identification of TCR and PD-1 as a link between AR and Aldo-salt-induced aortic aneurysms

Since LMT-28 completely inhibited the IL-6 signaling but only partially blocked Aldo-salt-induced aortic aneurysms (Figure 5), we hypothesized that additional signaling pathways regulated by androgen might be involved in Aldo-salt-induced aortic aneurysms. To identify these putative signaling ways in an unbiased way, 10-month-old male C57BL/6J mice were randomly divided into three groups: 1) Aldo-salt; 2) orchiectomy followed by Aldo-salt; 3) orchiectomy followed by Aldo-salt with DHT. Whole aortas were harvested one week after the Aldo-salt administration. Subsequently, these samples underwent RNA-seq for comprehensive gene expression analysis.

Of a total of 18,841 mRNAs detected by RNA-seq, DESeq2 (25) identified 2,359 of them as significantly and differentially abundant ($P < 0.01$) among aortas from the three groups of mice (Figure 6A). Orchiectomy caused the upregulation of 298 mRNAs and the downregulation of 351 mRNAs (Figure 6B). Conversely, administration of DHT to orchiectomized mice resulted in the upregulation of 707 mRNAs and the downregulation of 1,003 mRNAs (Figure 6C). Importantly, the rescue of androgen deprivation by DHT in orchiectomized mice identified 180 androgen-sensitive mRNAs upregulated by orchiectomy but downregulated by DHT (Figures 6D and 6E; Supplemental Table 1) and 150 androgen-sensitive mRNAs downregulated by orchiectomy but upregulated by DHT (Figures 6G and 6H; Supplemental Table 2).

To gain mechanistic insight into the androgen-sensitive mRNAs identified by the RNA-seq analysis, we employed Enrichr, a widely-used search engine for comprehensive pathway enrichment analysis (26), to unveil the signaling pathways responsive to androgen and potentially implicated in Aldo-salt-induced aortic aneurysms. Based on the 180 androgen-sensitive mRNAs upregulated by orchiectomy but downregulated by DHT (Figures 6D and 6E), Enrichr analysis revealed 65 overrepresented

functional annotations (Figure 6F and Supplemental Table 3). Surprisingly, most of these annotations were associated with adaptive immunity, particularly TCR signaling pathways, including PD-1 (Figure 6F and Supplemental Table 3). In parallel with this finding, the 150 androgen-sensitive mRNAs downregulated by orchiectomy but upregulated by DHT (Figures 6G and 6H) were pinpointed to 19 overrepresented functional annotations, most of which were associated with triglyceride, fatty acid, and lipid biosynthesis or metabolism (Figure 6I and Supplemental Table 4).

Among the TCR signaling pathways revealed by RNA-seq analysis, PD-1 is particularly interesting for several reasons. Firstly, there is little information regarding the regulation of PD-1 by androgens and its role in aortic aneurysms. Secondly, PD-1 is well-recognized for its pivotal role as an immune checkpoint in regulating T cells, immunity, and immune-based cancer therapy (11, 27, 28). Thirdly, PD-1 immune checkpoint therapy has been shown to have sex differences (29) and is associated with serious immune-related cardiovascular adverse events, including autoimmune myocarditis, pericarditis, and vasculitis (11, 27, 28). Consequently, it is conceivable that PD-1 may be involved in Aldo-salt-induced and androgen-mediated aortopathy. Therefore, our subsequent studies have been directed toward investigating PD-1 in greater depth.

RNA-seq revealed 180 androgen-response genes associated with TCR and PD-1 signaling pathways. However, it is plausible that the findings may arise from the differential composition of aortic cells rather than the specific activation of TCR and PD-1 signaling pathways. To discern these possibilities, we conducted flow cytometry analysis of T-cell subset signatures in the aortas of three groups of 10-month-old male WT C57BL/6J mice ten days after Aldo-salt with 1) sham operation, 2) orchiectomy, and 3) orchiectomy with DHT. As depicted in Supplemental Figures 14 and 15 for the gating strategy of flow cytometry analysis, single aortic cells were first gated on CD45 *vs.* live/dead cell staining to select viable leukocytes and then gated on CD3, CD4, and CD8 to identify total T-cells, CD4 T-cells, and CD8 T-cells, respectively. CD4 and CD8 T-cells were further gated on CD44,

CD62L, and CD127 to distinguish central memory T-cells (Tcm; $CD44^+CD62L^+$), naïve T-cells ($CD44^-CD62L^+$), effector T-cells (Teff; $CD44^+CD62L^-CD127^-$), and effector memory T-cells (Tem; $CD44^+CD62L^-CD127^+$), respectively. We selected these T-cell subsets based on our RNA-seq pathway enrichment analysis (Figure 6F). These T-cell subsets were also gated on PD-1 to pinpoint $PD\text{-}1^+$ T-cell subsets. As a control, a single-cell suspension from the spleen was analyzed by flow cytometry with fluorescence minus one (FMO) to define gating boundaries and ensure the specificity of antibodies.

Concurrently with TCR and PD-1 signaling pathways identified by RNA-seq analysis (Figures 6D−6F), the total numbers of all examined T-cell subsets exhibited a similar trend in response to orchiectomy and DHT: increased by orchiectomy but decreased by DHT (Supplemental Table 6). Consistent with these findings, several T-cell subsets, including CD4 T-cells, naïve CD4 T-cells, naïve CD8 T-cells, $PD\text{-}1^+$ CD4 Teff cells, and $PD\text{-}1^+$ CD4 Tcm cells, displayed a significant or trending percentage increase induced by orchiectomy and/or a percentage decrease elicited by DHT (Figure 7 and Supplemental Table 5). Intriguingly, in contrast to the total T-cell number response to orchiectomy and DHT, several other T-cell subsets exhibited a significant or trending percentage decrease induced by orchiectomy and/or a percentage increase elicited by DHT (Supplemental Table 5).

To trace the origins of T-cell subsets in the aorta, we analyzed T-cell subsets by flow cytometry in the spleens from the same three groups of mice. Interestingly, a similar effect of androgen on T-cell subsets was found in the spleens as in the aortas, although the total number but not the percentage of T-cell subsets were mostly affected (Supplemental Figure 16 and Supplemental Table 6), indicating that alterations in T-cell subsets within the spleen, induced by orchiectomy and/or DHT, contribute to the changes observed in T-cell subsets within the aorta.

Splenectomy mitigates Aldo-salt-induced aortic aneurysms and augments $PD\text{-}1^+$ T-cells and

PD-1$^+$ B-cells in the aorta

To explore the potential involvement of T-cells in Aldo-salt-induced aortic aneurysms,11-13-month-old male C57BL/6J mice were subjected to splenectomy or sham operation, and four weeks later, they received an additional four-week Aldo-salt administration. In line with previous findings (30), splenectomy lowered MAP before and after Aldo-salt administration (Figure 8A), indicating the effectiveness of splenectomy. Compared to sham operations, splenectomy suppressed Aldo-salt-induced suprarenal aortic dilation and progression (Figures 8B and 8C), the external diameters of the AscAo, ArchAo, and SupAo (Figure 8D), and the incidence of AAA, TAA, and aortic rupture (Figure 8E). Interestingly, a significant correlation was observed between MAP and the internal diameters of the suprarenal aorta of mice three weeks after Aldo-salt administration (Supplemental Figure 17A). However, there was no significant difference in MAP between splenectomized mice with and without aortic aneurysms (Supplemental Figure 17B).

To investigate whether PD-1$^+$ T-cells are implicated in the effect of splenectomy on Aldo-salt-induced aortic aneurysms, we conducted flow cytometry analysis of the aortas from splenectomized and sham-operated mice four weeks after Aldo-salt administration. As delineated in Supplemental Figure 18, single aortic cells were first gated on CD45 to sort leukocytes and then gated on CD3, CD19, F4/80, and Ly6G to identify T-cells, B-cells, macrophages, and neutrophils, respectively. These cells were further gated on PD-1 to identify PD-1$^+$ T cells, PD-1$^+$ B cells, PD-1$^+$ macrophages, and PD-1$^+$ neutrophils. Compared to sham operation, splenectomy did not affect the total numbers and percentages of leukocytes, T-cells, B-cells, macrophages, and neutrophils in the aorta of mice administered Aldo-salt (Supplemental Figure 19). However, splenectomy notably increased the percentages, albeit not the total numbers, of PD-1$^+$ T-cells and PD-1$^+$ B cells in the aorta of mice administered Aldo-salt (Figures 8F−8K). Conversely, splenectomy significantly decreased the percentages and total numbers of PD-1$^+$ neutrophils while not affecting PD-1$^+$ macrophages in the aorta of mice administered Aldo-salt (Supplemental Figures 20A−20F).

To trace the origins of PD-1$^+$ T-cell subsets in the aorta of splenectomized mice, we conducted flow cytometry analysis of the blood and periaortic lymph nodes in 11-13-month-old splenectomized and sham-operated mice four weeks after Aldo-salt administration. Interestingly, splenectomy did not alter the total number and percentage of leukocytes, T-cells, B-cells, PD-1$^+$ T-cells, and PD-1$^+$ B-cells in the blood compared to sham operation (Supplemental Figure 21). In contrast, splenectomy led to a notable increase in the total number, although not the percentage, of leukocytes, T-cells, B-cells, PD-1$^+$ T-cells, and PD-1$^+$ B-cells in the periaortic lymph nodes relative to sham operation (Supplemental Figure 22). These findings suggest that splenectomy may enrich PD-1$^+$ T-cells and PD-1$^+$ B-cells in the aortas via the periaortic lymph nodes.

AR binds to the PD-1 promoter and suppresses its mRNA and protein expression in the spleen

We conducted a series of experiments to investigate whether PD-1 is regulated by androgen in the spleen. Firstly, we examined PD-1 protein expression by IHC in the spleens from 10-month-old male C57BL/6J mice with orchiectomy or sham operation ten days after Aldo-salt administration. PD-1 protein was predominantly observed in the white pulp of the spleen (Figures 9A and 9B), a region primarily composed of T cells and B cells (31). Importantly, PD-1 protein expression was notably elevated by orchiectomy in the spleen relative to sham operation (Figures 9A and 9B). Consistent with these findings, DHT administration to orchiectomized mice abolished PD-1 protein upregulation in the spleen four weeks after Aldo-salt administration (Figures 9C and 9D).

Secondly, we quantified PD-1 protein expression by Western blots in the spleen of 10-month-old orchiectomized or sham-operated C57BL/6J mice ten days after Aldo-salt administration. PD-1 protein expression was markedly upregulated by orchiectomy up to 4-fold in the spleen compared to sham operation (Figures 9E and 9F). To discern whether orchiectomy-induced PD-1 protein upregulation in the spleen is attributed to T-cells or B-cells, we examined CD3ε, a T-cell marker, and

CD19, a B-cell marker, protein expressions in the same spleen lysate. Interestingly, both CD3ε and CD19 proteins showed a moderate increase in the spleen of orchiectomized mice compared to sham-operated mice, but only CD3ε protein upregulation was statistically significant (Figures 9E, 9G, and 9H).

We also investigated the effects of orchiectomy on PD-1, CD3ε, and CD19 protein expressions in the spleen of 10-month-old orchiectomized and sham-operated C57BL/6J mice without Aldo-salt administration. An increasing trend in PD-1, but not CD3ε and CD19, basal protein expression was observed in the spleens (Supplemental Figures 23). However, the level of PD-1 upregulation induced by orchiectomy in the spleen of the mice without Aldo-salt was notably lower than those with Aldo-salt (Supplemental Figures 23 *vs.* Figures 9E and 9F).

Thirdly, we conducted a flow cytometry analysis of the spleens from 10-month-old orchiectomized and sham-operated C57BL/6J mice ten days after Aldo-salt administration, to discern the upregulation of PD-1 protein, as detected by IHC and Western blots, in splenic T-cells or B-cells. Interestingly, orchiectomy significantly increased the total number, not the percentage, of splenic PD-1^+ T-cells, but not splenic PD-1^+ B-cells, compared to sham operation ten days after Aldo-salt administration (Supplemental Figures 24). These findings suggest that orchiectomy-induced PD-1 protein upregulation in the spleen mainly results from splenic PD-1^+ T-cells, rather than splenic PD-1^+ B-cells, in mice administered Aldo-salt.

Fourthly, to investigate whether splenic PD-1 is regulated by androgen at the transcription level, we determined Pdcd1 (the gene that codes PD-1) mRNA expression by real-time PCR in the spleen of 10-month-old male C57BL/6J mice with orchiectomy or sham operation ten days after Aldo-salt administration. Pdcd1 mRNA was significantly upregulated by orchiectomy in the spleen compared to sham operation (Figure 9I).

Fifthly, to investigate the mechanism by which androgen suppresses Pdcd1 mRNA expression in the spleen in mice administered Aldo-salt, we examined whether AR binds to the PD-1 promoter to suppress its transcription. We analyzed a 5-kb mouse PD-1 promoter DNA sequence to identify androgen response elements (AREs) containing AGAACA or TGTTCT hexamers, known to bind AR effectively (32). We found 12 putative AREs in the 5-kb mouse PD-1 promoter (Figure 9J). To determine whether AR can bind to these putative ARE in the spleen, we performed a ChIP assay using the mouse spleen samples with two commercially available ChIP-grade anti-AR Ab with distinct epitopes, along with two sets of ChIP-PCR primers specific for amplifying ARE4 and ARE6 in the mouse PD-1 promoter (Figure 9J). Both anti-AR Ab, but not the control Ab, successfully pulled down the chromatin fragments containing ARE6 but not ARE4 (Figures 9K−9M), indicating that AR can bind to the ARE6 but not ARE4 in the mouse PD-1 promoter in the spleen.

Sixthly, to investigate whether the binding of AR to the PD-1 promoter inhibits its transcriptional activity, we subcloned a 488 bp PD-1 mouse promoter (-4,444 to -3,956 bp relative to the transcription start site (TSS)) containing ARE6 to ARE10 (Figure 9J) into a pGL3-basic firefly luciferase report vector. The pGL3-basic-PD-1 promoter construct was co-transfected with the pRL-TK control vector and a pcDNA Flag-M4-AR construct (33) into HEK293 cells. Dual luciferase assays revealed that the -488 bp PD-1 promoter exhibited a 4.6-fold higher luciferase activity than the pGL3-basic vector (Figure 9O), indicating that the cloned -488 bp PD-1 promoter can drive PD-1 transcription. Importantly, co-transfection of the PD-1 promoter-luciferase constructs with the human AR cDNA construct completely abolished the PD-1 promoter activity in the presence of DHT (Figure 9O).

Seventhly, to investigate the link between orchiectomy-induced PD-1 upregulation in the spleen and Aldo-salt-induced aortic aneurysms, we conducted a flow cytometry analysis of the blood of 10-

month-old orchiectomized and sham-operated C57BL/6J mice ten days after Aldo-salt administration. In line with its effect on PD-1$^+$ T-cells and PD-1$^+$ B-cells in the spleen (Supplemental Figures 24), orchiectomy amplified both the total and percentage of PD-1$^+$ T-cells in the blood, though it did not affect PD-1$^+$ B-cells (Supplemental Figures 25).

Eighthly, to investigate whether orchiectomy-induced PD-1 upregulation also occurs in other immune organs, we examined PD-1 protein expression by IHC and Western blot analysis in the periaortic lymph nodes of 10-month-old orchiectomized and sham-operated C57BL/6J mice ten days after Aldo-salt administration. IHC analysis showed a discernible increasing trend in PD-1 immunostaining in the periaortic lymph nodes of orchiectomized mice compared to sham-operated mice (Supplemental Figures 26A and 26B). This observation was further supported by Western blot analysis (Supplemental Figures 26C and 26D).

Finally, to ascertain whether PD-1 regulates IL-6 in T cells, we assessed IL-6 mRNA and protein expressions in the spleen of 4-month-old male global PD-1 knockout (34) and WT C57BL/6J mice received 8-week HFD feeding and 4-week Ang II infusion (35). There were no significant differences in IL-6 mRNA and protein expressions in the spleen between PD-1 KO and WT mice (Supplemental Figure 27A−27E). Consistent with these findings, there was no significant difference in serum IL-6 protein levels between PD-1 KO and WT mice (Supplemental Figure 27F).

Blockade of the immune checkpoint with anti-PD-1 Ab reinstates Aldo-salt-induced aortic aneurysms in orchiectomized mice

To explore the potential role of PD-1 in Aldo-salt-induced and androgen-mediated aortic aneurysms, 10-month-old C57BL/6J male mice underwent orchiectomy and then administered Aldo-salt with a specific rat anti-mouse PD-1 Ab or an isotype control Ab (200 μg/mice, i.p. injection, twice a week) for eight weeks (36). Compared to the control Ab, anti-PD-1 Ab significantly enhanced suprarenal aortic

dilation from week four to week eight (Figure 10A). A similar but more potent effect of anti-PD-1 Ab was found on Aldo-salt-induced aortic arch dilation from week six to week eight after Aldo-salt with anti-PD-1 or control Ab administration (Figure 10B). Additionally, anti-PD-1 Ab significantly increased the external diameters of the AscAo, ArchAo, DesAo, and SupAo relative to the control Ab (Figure 10C). Moreover, of 12 mice with anti-PD-1 Ab, 5 developed aortic aneurysms (45%), including 1 AAA (8%), 5 TAA (45%), and 1 aortic rupture (8%). In contrast, none of 8 mice with the control Ab developed aortic aneurysms (Figure 10D).

The aortas were harvested from orchiectomized mice eight weeks after Aldo-salt with anti-PD-1 or control Ab administration and then subjected to Verhoeff-Van Gieson staining (9, 10) to examine the effect of anti-PD-1 Ab on Aldo-salt-induced aortic elastin fiber fragmentation. A noticeable increase in the breakage of thoracic and abdominal aortic elastin fiber was evident in orchiectomized mice with aortic aneurysms induced by anti-PD-1 Ab, but not in mice administered with control Ab without aortic aneurysms (Figures 10E−10G). The same thoracic aortas also underwent IHC with anti-CD3ε, CD19, F4/80, and Ly6G Ab to identify T-cells, B-cells, macrophages, and neutrophils, respectively. As depicted in Figure 10H, T cells, B cells, macrophages, and neutrophils were prominently present in the thoracic aorta of mice with TAA induced by anti-PD-1 Ab, whereas they were barely detectable in mice administered with control Ab without TAA.

Interestingly, anti-PD-1 Ab did not affect MAP before and three weeks after Aldo-salt administration, but it exacerbated Aldo-salt-induced hypertension seven weeks after Aldo-salt administration (Figure 10I). There was a significant correlation between the internal diameters of the aortic arch and MAP seven weeks after Aldo-salt administration (Supplemental Figure 28A). However, there was no significant difference in MAP between orchiectomized mice treated with the anti-PD-1 Ab regardless of whether they developed aortic aneurysms (Supplemental Figure 28B).

To explore the potential involvement of PD-1 in human aortic aneurysms, we examined PD-1 protein expression by IHC in the abdominal aorta specimens from human patients with or without AAA. PD-1 protein was scarcely detectable in normal abdominal aortas but was readily found in human AAA (Figures 10J and 10K).

Adoptive PD-1 deficient T-cell transfer resumes Aldo-salt-induced aortopathy in orchiectomized mice

To further define the role of PD-1 in the pathogenesis of Aldo-salt-induced aortic aneurysms, PD-1 deficient T-cells and WT T-cells were isolated by microbeads conjugated with a monoclonal anti-mouse CD90.2 Ab from the spleens of 4-5-month-old male PD-1-KO and WT C57BL6J donor mice and then adoptively transferred to 9-10-month-old orchiectomized C57BL/6J recipient mice via retro-orbital sinus injection two days before and eight and eighteen days after Aldo-salt administration. Pilot experiments confirmed the presence of adoptively transferred T cells preloaded with a red fluorescent cell tracker in the recipient mice's spleen and aorta (Gong and Guo, unpublished observation).

Compared to mice receiving WT T-cells, those with adoptive PD-1 deficient T-cell transfer displayed a significantly greater suprarenal aortic and aortic root (RootAo) dilation following Aldo-salt administration (Figures 11A and 11B). Consistent with these findings, the aorta weight to BW ratio, an index of aortic aneurysm severity (5), but not the spleen weight to BW ratio, also exhibited a significant increase in mice with adoptive PD-1 deficient T-cell transfer compared to those with adoptive WT T-cell transfer (Figures 11C and Supplemental Figures 29). Additionally, adoptive PD-1 deficient T-cell transfer, relative to adoptive WT T-cell transfer, led to a significant increase in the external diameters of the RootAo, AscAo, and SupAo four weeks after Aldo-salt administration (Figure 11D), along with 60% TAA, 10% AAA, 40% aortic rupture (Figure 11E). In contrast, none of the mice receiving adoptive WT T-cell transfer developed TAA, AAA, and aortic rupture.

Mice receiving PD-1 deficient T-cells developed TAA, characterized by evident elastin fiber breakages (Figures 11F and 11G) and prominent infiltration of T-cells, macrophages, and neutrophils, but not B-cells, in the thoracic aortas compared to those with WT T-cell transfer without TAA (Figure 11H). However, adoptive PD-1 deficient T-cell transfer did not affect MAP before and after Aldo-salt administration (Figure 11I). No significant correlation was found between MAP and aortic root dilation in mice receiving PD-1 deficient and WT T-cell transfer three weeks after Aldo-salt administration (Figure 11J). Furthermore, there was no significant difference in MAP between mice with PD-1 deficient and WT T-cell transfer, regardless of mice with aortic aneurysms (Figure 11K).

Genetic deletion of PD-1 exacerbates HFD and Ang II-induced AAA in non-orchiectomized mice

To investigate whether PD-1 is implicated in other aortic aneurysm animal models, 2-month-old male PD-1-KO and WT C57BL/6J mice (34) were fed an HFD for one month and then infused with Ang II in the continued presence of HFD feeding for an additional month to induce AAA (35). HFD and Ang II, but not HFD alone, result in both abdominal and thoracic aortic dilaton, and importantly, genetic deletion of PD-1 exacerbated HFD and Ang II-induced aortic dilation, with a more pronounced effect observed in the SupAo than the RootAo (Figures 12 A and 12B). In line with these findings, PD-1-KO mice also exhibited a significant increase in the aorta weight to BW ratio (Figure 12C and Supplemental Figure 30A), external diameters of the AscAo, ArchAo, DesAo, and SupAo (Figure 12D), and the incidence of aortic aneurysms, mainly AAA rather than TAA, which was different from those in orchiectomized mice with Aldo-salt (Figures 12E *vs.* 10D and 11E).

Interestingly, genetic deletion of PD-1 did not affect BW four weeks after HFD feeding or HFD feeding plus Ang II infusion (Supplemental Figure 30B). However, genetic deletion of PD-1 significantly increased spleen weight and the spleen weight to BW ratio, but no kidney weight and the kidney weight to BW ratio (Supplemental Figures 30C−30F), indicating the involvement of immune cells.

Consistent with these findings, genetic deletion of PD-1 amplified HFD and Ang II-induced elastin fiber fragmentation and infiltration of T-cells, B-cells, macrophages, and neutrophils in the suprarenal aorta compared to WT mice (Figures 12F−12H).

Genetic deletion of PD-1 did not affect MAP before and after HFD feeding and Ang II infusion (Figure 12I). There was no significant correlation between MAP and the internal diameters of the suprarenal aorta in PD-1 KO and WT mice three weeks after HFD and Ang II administration (Figure 12J). Furthermore, there was no significant difference in MAP between PD-1 KO and WT mice, regardless of whether they developed AAA (Figure 12K).

Discussion

It has long been recognized that androgen plays a role in cardiovascular diseases (37). However, whether androgen protects or aggravates aortic aneurysms remains inconclusive and appears to be animal model-specific (5-7, 16, 38). In this study, we report that Aldo-salt-induced aortic aneurysms mimicked human AAA (3) and mostly occurred in male but not female mice (Figure 1). Consistent with the Ang II and elastase AAA mouse models (5, 7, 16) but not the Ang II plus $CaCl_2$ mouse model (38), we demonstrate that Aldo-salt-induced aortic aneurysms were abolished or ameliorated by global androgen deprivation via orchiectomy (Figure 2), downregulation of AR with ASC-J9 (Figure 4), and inhibition of AR with flutamide (Supplemental Figure 8). Importantly, restoration of androgen in orchiectomized mice reinstated Aldo-salt-induced aortic aneurysms (Figure 3).

One of the most important findings is that androgen aggravates Aldo-salt-induced aortic aneurysms, at least partially, via suppressing PD-1^+ T cells in the spleen. Several lines of evidence support this potential mechanism. Firstly, RNA-seq identified 180 genes upregulated by orchiectomy but downregulated by DHT in the aortas of mice one week after Aldo-salt administration (Figures 6D and 6E and Supplemental Tables 1). Surprisingly, these 180 androgen-sensitive genes were mostly mapped to the TCR signaling, including PD-1 (Figure 6F and Supplemental Tables 3), and importantly, these findings were largely confirmed by flow cytometry (Figure 7 and Supplemental Table 5). Secondly, consistent with the potential role of T-cells in AAA (39-41), splenectomy mitigated Aldo-salt-induced aortic aneurysms (Figures 8A−8E), accompanied by the enrichment of PD-1^+ T- and PD-1^+ B-cells in the aorta of mice administered Aldo-salt, probably via the periaortic lymph nodes (Figures 8F−8K; Supplemental Figures 18−22). Thirdly, orchiectomy potently augmented PD-1^+ T-cells but not PD-1^+ B-cells in the spleen, blood, and lymph nodes of mice administered Aldo-salt (Figures 9A−9H and Supplemental Figures 24−26). Finally, immune checkpoint blockade with anti-PD-1 Ab, adoptive PD-1 deficient T-cell transfers, and genetic deletion of PD-1 reinstates or exacerbates Aldo-salt- or HFD and Ang II-induced aortopathies, including elastin degradation,

vascular inflammation, TAA, and AAA in intact and orchiectomized mice (Figures 10−12). These findings align well with the established role of PD-1$^+$ T-cells as an immune checkpoint implicated in various diseases, including giant cell arteritis, cancer, and atherosclerosis (28). However, it should be noted that these findings contradict a recent study where humanized PD-1 Ab mitigates rather than aggravates AAA in the $CaCl_2$ mouse model and aortic patch angioplasty rat model (42). The discrepancy between these studies may be attributed to differences in animal models, animal age, and anti-PD-1 Ab. Further studies are needed to investigate these possibilities.

PD-1 functions as an immune checkpoint, inhibiting T-cell activation via interaction with its ligand, primarily PD-L1 (28). PD-1 is exclusively expressed in activated immune cells, most importantly in T cells, whereas PD-L1 is broadly expressed in various cells, including antigen-presenting cells (i.e., macrophages), cancer cells, and endothelial cells (28). It is well-documented that PD-1 is upregulated by estrogen in Tregs, B-cells, macrophages, and dendritic cells (43). However, whether androgen can modulate PD-1 expression is largely unknown. As a result, the mechanism by which androgen suppresses PD-1 expression is completely unknown. One of what we believe to be novel findings is that we unrevealed a mechanism by which androgen suppresses PD-1 expression in the spleen. Specifically, we demonstrated that AR bound to the PD-1 promoter via ARE, suppressing its transcription, mRNA, and protein expression in the spleen (Figure 9 and Supplemental Figure 23).

Given that androgen exerts a pleiotropic effect on various organs and systems through both genomic and non-genomic mechanisms (37), it is conceivable that androgen aggravates Aldo-salt-induced aortic aneurysms through multiple mechanisms. Consistent with this notion, it has been shown that androgen exacerbates Ang II-induced AAA through Ang II-type-1A receptor, IL-1α, and TGFβ1 (6, 16). The current study identified 65 signaling pathways downregulated and 19 signaling pathways upregulated by androgen in the aorta following Aldo-salt administration (Figure 6 and Supplemental Tables 1−4). While the role of these signaling pathways in Aldo-salt-induced aortic aneurysms

remains to be investigated, we demonstrate that IL-6, a pleiotropic cytokine, along with PD-1, is implicated in Aldo-salt-induced aortic aneurysms (Figure 5 and Supplemental Figures 9 and 10). It has been shown that IL-6 augments TCR-induced PD-1 expression via STAT3 and STAT4 in splenic T-cells (44). However, it is unlikely that PD-1 regulates IL-6 expression in splenic T cells as genetic deletion of PD-1 does not affect IL-6 expression in the spleen and serum of mice administered HFD feeding and Ang II infusion (Supplemental Figure 27). Thus, further investigation is warranted to define how PD-1 and IL-6 coordinate to mediate Aldo-salt-induced and androgen-mediated aortic aneurysms.

The current studies have several limitations. Firstly, most experiments were conducted in mice administered Aldo-salt, lacking a control group without Aldo-salt administration. Consequently, how the Aldo/MR signaling coordinates with the androgen/AR signaling in regulating PD-1 expression in T cells and aortic aneurysms remains unclear. Secondly, the current studies exclusively focused on the TCR and PD-1 signaling pathways resulting from 180 androgen-response genes in the aorta, neglecting exploration of the potential role of metabolic pathways enriched from 150 androgen-response genes in Aldo-salt-induced aortic aneurysms. Thirdly, LMT-28 may have potential off-targets relative to inhibiting IL-6. Addressing these limitations in future studies will contribute to a more comprehensive understanding of the mechanisms by which androgen aggravates aortic aneurysms.

Given that immune checkpoint inhibitors (i.e., anti-PD-1 Ab) have been successful in cancer treatment and have revolutionized the cancer research field (11), an increasing number of cancer patients have been subjected to immune checkpoint therapy (27). However, immune checkpoint therapy is associated with serious immune-related cardiovascular adverse events, including autoimmune myocarditis, pericarditis, and vasculitis (27). In alignment with these findings, the current studies suggest an increased risk of developing aortic aneurysms for patients undergoing

immune checkpoint inhibitor therapy. Indeed, a recent case report shows that a 57-year-old man with lung adenocarcinoma treated with chemotherapy and immune checkpoint blockade developed inflammatory TAA (45). Thus, cancer patients predisposed to the risk factors of aortic aneurysms, such as being male, aging, and smoking, may have an increased likelihood of developing aortic aneurysms during immune checkpoint therapy. As a precaution, these patients should be advised to undergo an ultrasound screen for aortic aneurysms to increase the life-saving potential of cancer immunotherapy.

Methods

Detailed materials and methods are provided in Supplemental Material.

Sex as a biological variable

Our study examined male and female animals, and sex-dimorphic effects were reported. Human aortic samples were obtained from male subjects.

Statistical analysis

All data were expressed as mean ± SEM. To compare one parameter between the two groups, normality tests were conducted. If data passed the normality test, a parametric, unpaired, and two-tailed t-test was employed. If data did not pass the normality test, a nonparametric, unpaired, and two-tailed test was used. For multiple comparisons of two parameters among multiple groups, a two-way ANOVA was performed with correction for multiple comparisons by controlling the false discovery rate. Similarly, for multiple comparisons of three parameters among multiple groups, a three-way ANOVA was used with correction for multiple comparisons by controlling the false discovery rate. The incidence of aortic aneurysms between the two groups was compared using a two-sided Chi-Square test. The relationship between two quantitative variables was analyzed through simple linear regression. Significant outliers, identified by the outlier calculator (GraphPad), were excluded from the statistical analysis. All statistical analysis was carried out using Prism 9 software (GraphPad). A *P*-value or adjusted *P*-value < 0.05 was considered significant unless specified somewhere. A *P*-value of > 0.05 was considered not significant (ns).

Study approval

All animal procedures were approved by the Institutional Animal Care and Use Committee of the University of Kentucky. All procedures for using human aortic aneurysm specimens for the current study were approved by the Institutional Review Board of the University of Kentucky.

Data availability

RNA-seq data were deposited into the NCBI's Gene Expression Omnibus database under accession number GSE255682. Values for all data points in graphs are reported in the Supporting Data Values file. Requests for materials should be directed to the corresponding authors and will be fulfilled upon completion of appropriate material transfer agreements.

Author contributions

X.M., S.L., Z.W., and K.J.: contributed to designing research studies, conducting experiments, acquiring data, and analyzing data; T.M, A.S, and A. T. contributed to analyzing RNA-seq data; E.L. and J.C. contributed to providing human aortic aneurysm specimens; M.G. and Z.G. contributed to the conceptualization, supervision, writing, project administration, and funding acquisition.

Acknowledgments

This work is supported in part by the US NIH Grants HL125228, HL141103, HL142973, HL164398, and HL166225 (to M.G. and Z.G.), VA Merit Award CX001683 (to E.L. and Z.G.), R01 DC014468 and K18 DC014050 (to T.M.), the Institutional Development Award from the US National Institute of General Medical Sciences of NIH P30GM127211 (to the University of Kentucky Center of Research in Obesity & Cardiovascular Disease), and the Office of the Vice President for Research and an NIH NCI Center Core Support Grant P30 CA177558 (to the University of Kentucky Markey Cancer Center and Flow Cytometry & Immune Monitoring Core Facility).

References

1. Isselbacher EM. Thoracic and abdominal aortic aneurysms. *Circulation.* 2005;111(6):816-28.
2. Kent KC. Clinical practice. Abdominal aortic aneurysms. *N Engl J Med.* 2014;371(22):2101-8.
3. Golledge J, Muller J, Daugherty A, and Norman P. Abdominal aortic aneurysm: pathogenesis and implications for management. *Arterioscler Thromb Vasc Biol.* 2006;26(12):2605-13.
4. Robinet P, Milewicz DM, Cassis LA, Leeper NJ, Lu HS, and Smith JD. Consideration of Sex Differences in Design and Reporting of Experimental Arterial Pathology Studies-Statement From ATVB Council. *Arterioscler Thromb Vasc Biol.* 2018;38(2):292-303.
5. Henriques TA, Huang J, D'Souza SS, Daugherty A, and Cassis LA. Orchidectomy, but not ovariectomy, regulates angiotensin II-induced vascular diseases in apolipoprotein E-deficient mice. *Endocrinology.* 2004;145(8):3866-72.
6. Henriques T, Zhang X, Yiannikouris FB, Daugherty A, and Cassis LA. Androgen increases AT1a receptor expression in abdominal aortas to promote angiotensin II-induced AAAs in apolipoprotein E-deficient mice. *Arterioscler Thromb Vasc Biol.* 2008;28(7):1251-6.
7. Cho BS, Woodrum DT, Roelofs KJ, Stanley JC, Henke PK, and Upchurch GR, Jr. Differential regulation of aortic growth in male and female rodents is associated with AAA development. *J Surg Res.* 2009;155(2):330-8.
8. McCurley A, and Jaffe IZ. Mineralocorticoid receptors in vascular function and disease. *Mol Cell Endocrinol.* 2012;350(2):256-65.
9. Liu S, Xie Z, Daugherty A, Cassis LA, Pearson KJ, Gong MC, et al. Mineralocorticoid receptor agonists induce mouse aortic aneurysm formation and rupture in the presence of high salt. *Arterioscler Thromb Vasc Biol.* 2013;33(7):1568-79.
10. Lutshumba J, Liu S, Zhong Y, Hou T, Daugherty A, Lu H, et al. Deletion of BMAL1 in Smooth Muscle Cells Protects Mice From Abdominal Aortic Aneurysms. *Arterioscler Thromb Vasc Biol.* 2018;38(5):1063-75.

11. Sharma P, and Allison JP. Immune checkpoint targeting in cancer therapy: toward combination strategies with curative potential. *Cell.* 2015;161(2):205-14.
12. Daugherty A, Manning MW, and Cassis LA. Antagonism of AT2 receptors augments angiotensin II-induced abdominal aortic aneurysms and atherosclerosis. *Br J Pharmacol.* 2001;134(4):865-70.
13. Chaikof EL, Dalman RL, Eskandari MK, Jackson BM, Lee WA, Mansour MA, et al. The Society for Vascular Surgery practice guidelines on the care of patients with an abdominal aortic aneurysm. *J Vasc Surg.* 2018;67(1):2-77 e2.
14. Lee DL, Sturgis LC, Labazi H, Osborne JB, Jr., Fleming C, Pollock JS, et al. Angiotensin II hypertension is attenuated in interleukin-6 knockout mice. *Am J Physiol Heart Circ Physiol.* 2006;290(3):H935-40.
15. Gubbels Bupp MR, and Jorgensen TN. Androgen-Induced Immunosuppression. *Front Immunol.* 2018;9:794.
16. Huang CK, Luo J, Lai KP, Wang R, Pang H, Chang E, et al. Androgen receptor promotes abdominal aortic aneurysm development via modulating inflammatory interleukin-1alpha and transforming growth factor-beta1 expression. *Hypertension.* 2015;66(4):881-91.
17. Yang Z, Chang YJ, Yu IC, Yeh S, Wu CC, Miyamoto H, et al. ASC-J9 ameliorates spinal and bulbar muscular atrophy phenotype via degradation of androgen receptor. *Nature medicine.* 2007;13(3):348-53.
18. Lin TH, Izumi K, Lee SO, Lin WJ, Yeh S, and Chang C. Anti-androgen receptor ASC-J9 versus anti-androgens MDV3100 (Enzalutamide) or Casodex (Bicalutamide) leads to opposite effects on prostate cancer metastasis via differential modulation of macrophage infiltration and STAT3-CCL2 signaling. *Cell Death Dis.* 2013;4(8):e764.
19. Davis JP, Salmon M, Pope NH, Lu G, Su G, Meher A, et al. Pharmacologic blockade and genetic deletion of androgen receptor attenuates aortic aneurysm formation. *J Vasc Surg.* 2016;63(6):1602-12 e2.

20. Abbass A, D'Souza J, Khalid S, Asad-Ur-Rahman F, Limback J, Burt J, et al. Liddle Syndrome in Association with Aortic Dissection. *Cureus.* 2017;9(5):e1225.
21. Lindsay ME, and Dietz HC. Lessons on the pathogenesis of aneurysm from heritable conditions. *Nature.* 2011;473(7347):308-16.
22. Harrison SC, Smith AJ, Jones GT, Swerdlow DI, Rampuri R, Bown MJ, et al. Interleukin-6 receptor pathways in abdominal aortic aneurysm. *Eur Heart J.* 2013;34(48):3707-16.
23. Hong SS, Choi JH, Lee SY, Park YH, Park KY, Lee JY, et al. A Novel Small-Molecule Inhibitor Targeting the IL-6 Receptor beta Subunit, Glycoprotein 130. *J Immunol.* 2015;195(1):237-45.
24. Naamneh Elzenaty R, du Toit T, and Fluck CE. Basics of androgen synthesis and action. *Best Pract Res Clin Endocrinol Metab.* 2022;36(4):101665.
25. Love MI, Huber W, and Anders S. Moderated estimation of fold change and dispersion for RNA-seq data with DESeq2. *Genome Biol.* 2014;15(12):550.
26. Chen EY, Tan CM, Kou Y, Duan Q, Wang Z, Meirelles GV, et al. Enrichr: interactive and collaborative HTML5 gene list enrichment analysis tool. *BMC Bioinformatics.* 2013;14:128.
27. Zhang L, Reynolds KL, Lyon AR, Palaskas N, and Neilan TG. The Evolving Immunotherapy Landscape and the Epidemiology, Diagnosis, and Management of Cardiotoxicity: JACC: CardioOncology Primer. *JACC CardioOncol.* 2021;3(1):35-47.
28. Weyand CM, Berry GJ, and Goronzy JJ. The immunoinhibitory PD-1/PD-L1 pathway in inflammatory blood vessel disease. *J Leukoc Biol.* 2018;103(3):565-75.
29. Conforti F, Pala L, Pagan E, Corti C, Bagnardi V, Queirolo P, et al. Sex-based differences in response to anti-PD-1 or PD-L1 treatment in patients with non-small-cell lung cancer expressing high PD-L1 levels. A systematic review and meta-analysis of randomized clinical trials. *ESMO Open.* 2021;6(5):100251.
30. Perrotta M, Lori A, Carnevale L, Fardella S, Cifelli G, Iacobucci R, et al. Deoxycorticosterone acetate-salt hypertension activates placental growth factor in the spleen to couple sympathetic drive and immune system activation. *Cardiovasc Res.* 2018;114(3):456-67.

31. Lewis SM, Williams A, and Eisenbarth SC. Structure and function of the immune system in the spleen. *Sci Immunol.* 2019;4(33).
32. Massie CE, Adryan B, Barbosa-Morais NL, Lynch AG, Tran MG, Neal DE, et al. New androgen receptor genomic targets show an interaction with the ETS1 transcription factor. *EMBO Rep.* 2007;8(9):871-8.
33. Chen S, Gulla S, Cai C, and Balk SP. Androgen receptor serine 81 phosphorylation mediates chromatin binding and transcriptional activation. *J Biol Chem.* 2012;287(11):8571-83.
34. Keir ME, Freeman GJ, and Sharpe AH. PD-1 regulates self-reactive CD8+ T cell responses to antigen in lymph nodes and tissues. *J Immunol.* 2007;179(8):5064-70.
35. Police SB, Thatcher SE, Charnigo R, Daugherty A, and Cassis LA. Obesity promotes inflammation in periaortic adipose tissue and angiotensin II-induced abdominal aortic aneurysm formation. *Arterioscler Thromb Vasc Biol.* 2009;29(10):1458-64.
36. Koga N, Suzuki J, Kosuge H, Haraguchi G, Onai Y, Futamatsu H, et al. Blockade of the interaction between PD-1 and PD-L1 accelerates graft arterial disease in cardiac allografts. *Arterioscler Thromb Vasc Biol.* 2004;24(11):2057-62.
37. Lucas-Herald AK, Alves-Lopes R, Montezano AC, Ahmed SF, and Touyz RM. Genomic and non-genomic effects of androgens in the cardiovascular system: clinical implications. *Clin Sci (Lond).* 2017;131(13):1405-18.
38. Son BK, Kojima T, Ogawa S, and Akishita M. Testosterone inhibits aneurysm formation and vascular inflammation in male mice. *J Endocrinol.* 2019;241(3):307-17.
39. Xiong W, Zhao Y, Prall A, Greiner TC, and Baxter BT. Key roles of CD4+ T cells and IFN-gamma in the development of abdominal aortic aneurysms in a murine model. *J Immunol.* 2004;172(4):2607-12.
40. Sharma AK, Lu G, Jester A, Johnston WF, Zhao Y, Hajzus VA, et al. Experimental abdominal aortic aneurysm formation is mediated by IL-17 and attenuated by mesenchymal stem cell treatment. *Circulation.* 2012;126(11 Suppl 1):S38-45.

41. Ait-Oufella H, Wang Y, Herbin O, Bourcier S, Potteaux S, Joffre J, et al. Natural regulatory T cells limit angiotensin II-induced aneurysm formation and rupture in mice. *Arterioscler Thromb Vasc Biol.* 2013;33(10):2374-9.

42. Sun P, Zhang L, Gu Y, Wei S, Wang Z, Li M, et al. Immune checkpoint programmed death-1 mediates abdominal aortic aneurysm and pseudoaneurysm progression. *Biomed Pharmacother.* 2021;142:111955.

43. Dinesh RK, Hahn BH, and Singh RP. PD-1, gender, and autoimmunity. *Autoimmun Rev.* 2010;9(8):583-7.

44. Austin JW, Lu P, Majumder P, Ahmed R, and Boss JM. STAT3, STAT4, NFATc1, and CTCF regulate PD-1 through multiple novel regulatory regions in murine T cells. *J Immunol.* 2014;192(10):4876-86.

45. Ninomiya R, Kinehara Y, Tobita S, Konaka H, Jokoji R, Shintani T, et al. Inflammatory Thoracic Aortic Aneurysm in a Patient with Advanced Lung Adenocarcinoma Treated with Pembrolizumab. *Intern Med.* 2022;61(15):2339-41.

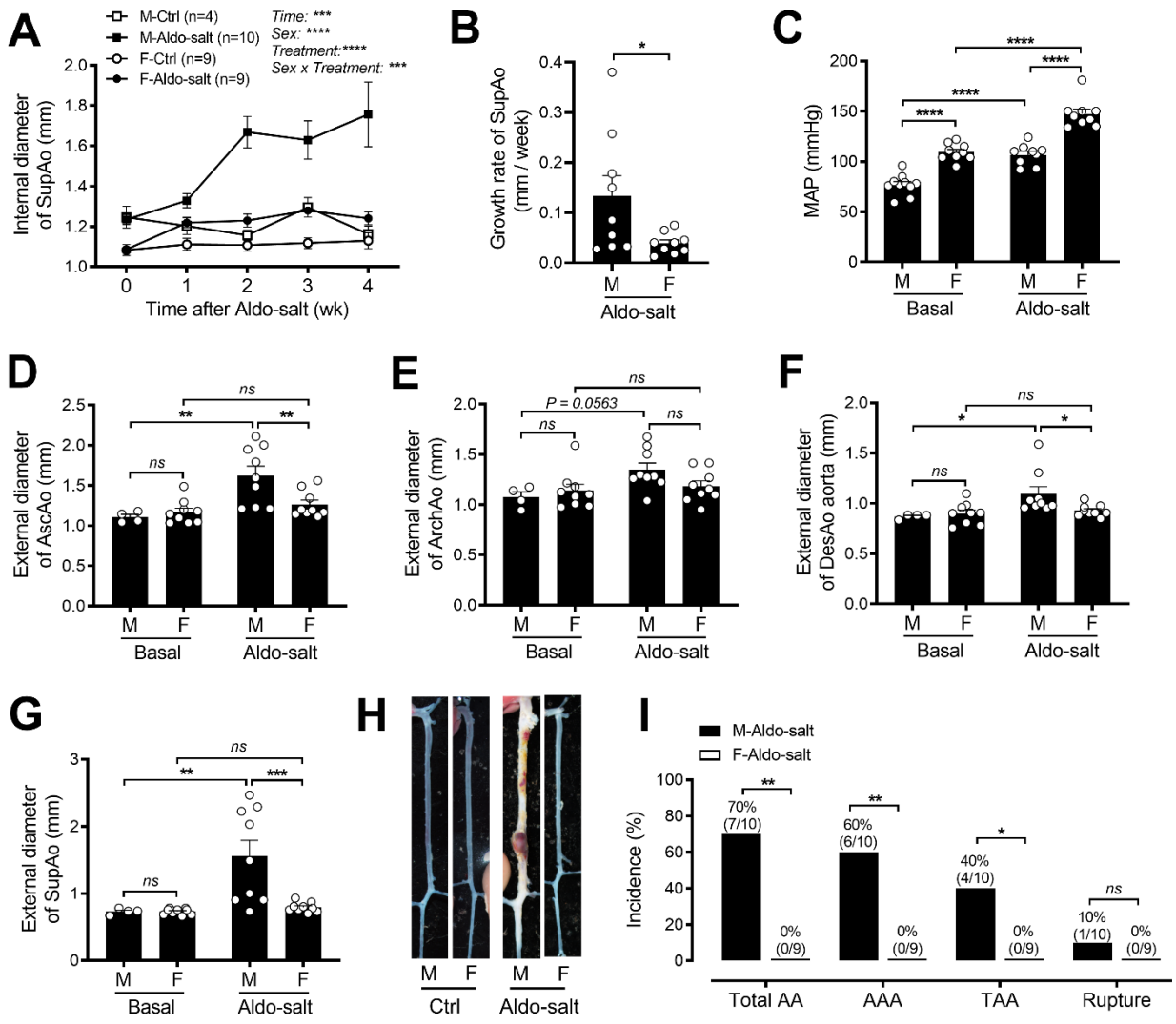

Figure 1. Sexual dimorphism in Aldo-salt-induced aortic aneurysms. (**A** and **B**) Maximal internal diameters and growth rate of the suprarenal aortas were measured weekly *in vivo* using ultrasound in 10-month-old male (M) and female (F) C57BL/6J mice administered Aldo-salt. Time 0 represents measurements one week before Aldo-salt administration (n = 4-10/group). (**C**) Mean arterial pressure (MAP) was measured via tail cuff in mice one week before (basal) and three weeks after Aldo-salt administration (n = 9-10/group). (**D−G**) Maximal external diameters of the ascending aorta (AscAo), aortic arch (ArchAo), descending aorta (DesAo), and suprarenal aorta (SupAo) were measured *ex vivo* by microscopy four weeks after Aldo-salt administration (n = 4-9/group). (**H**) Representative photographs of the aortas with or without aortic aneurysms. (**I**) Incidences of total aortic aneurysms (AA), abdominal aortic aneurysms (AAA), thoracic aortic aneurysms (TAA), and aortic rupture (mice with aortic aneurysms / mice with and without aortic aneurysms). Data were expressed as mean ± SEM and analyzed by thee-way ANOVA analysis (**A**), two-tailed unpaired *t*-test (**B**), two-way ANOVA with multiple comparison tests (**C−G**), and two-sided Chi-square test (**I**). **, P < 0.05; **, P < 0.01; ***, P < 0.001; ****, P < 0.0001; ns, not significant.*

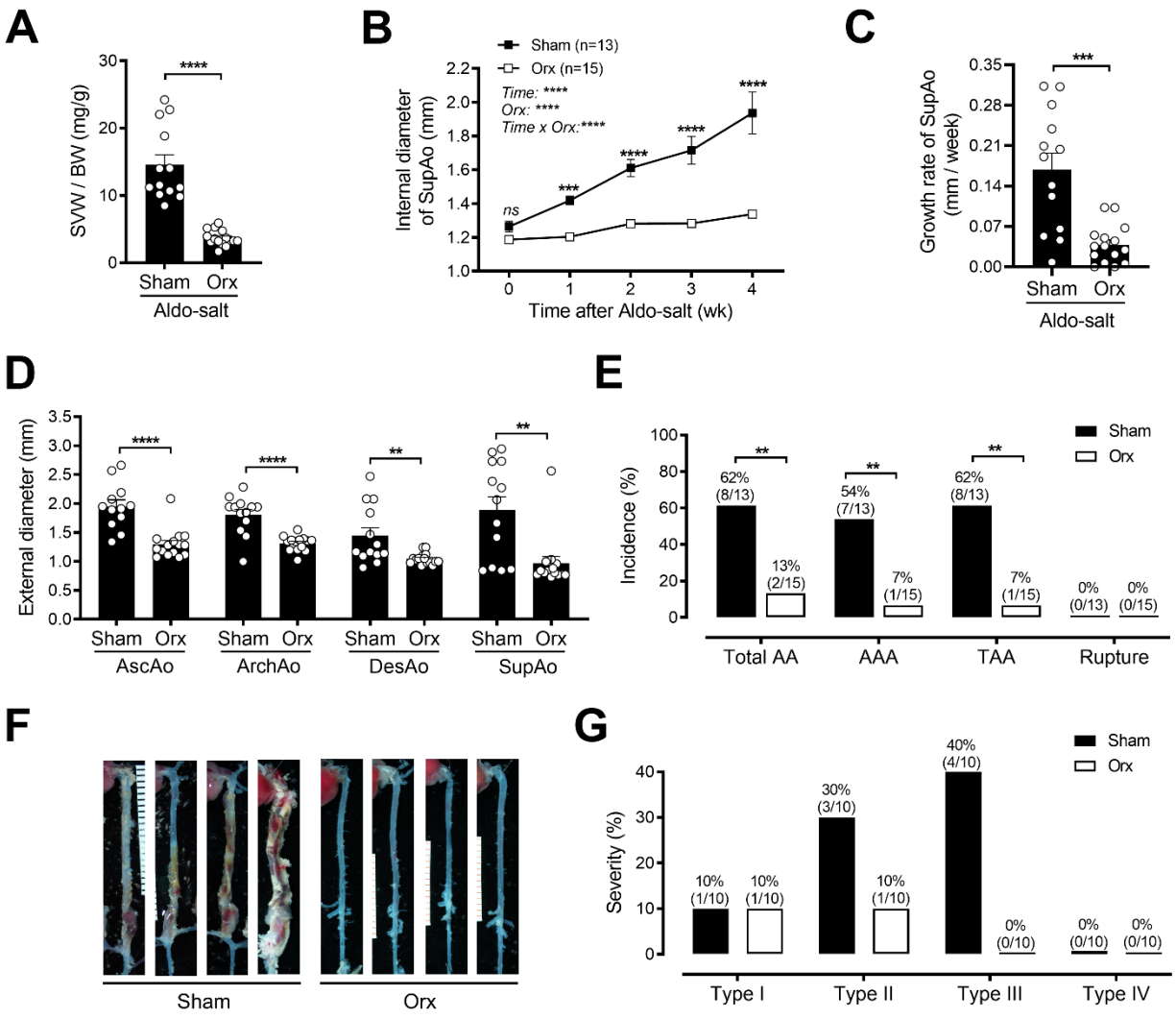

Figure 2. Orchiectomy protects mice from Aldo-salt-induced aortic dilation, progression, and aneurysm formation. (**A**) Seminal vesicle weight (SVW) to BW ratio was determined in orchiectomies (orx) and sham-operated 10-month-old male C57BL/6J mice four weeks after Aldo-salt administration (n = 13-15/group). (**B** and **C**) Maximal internal diameters and growth rate of the suprarenal aorta (n = 13-15/group). (**D**) Maximal external diameters of the AscAo, ArchAo, DesAo, and SupAo (n = 12-15/group). (**E**) Incidences of total AA, AAA, TAA, and aortic rupture. (**F**) Representative photographs of the aortas with and without aortic aneurysms. (**G**) Severity of aortic aneurysms (Supplemental Figure 3). Data were expressed as mean ± SEM and analyzed by two-tailed unpaired *t*-test (**A**, **C**, **D**), two-way ANOVA with multiple comparison tests (**B**), and two-sided Chi-square test (**E**). ***, P < 0.01; ***, P < 0.001; ****, P < 0.0001; ns, not significant.*

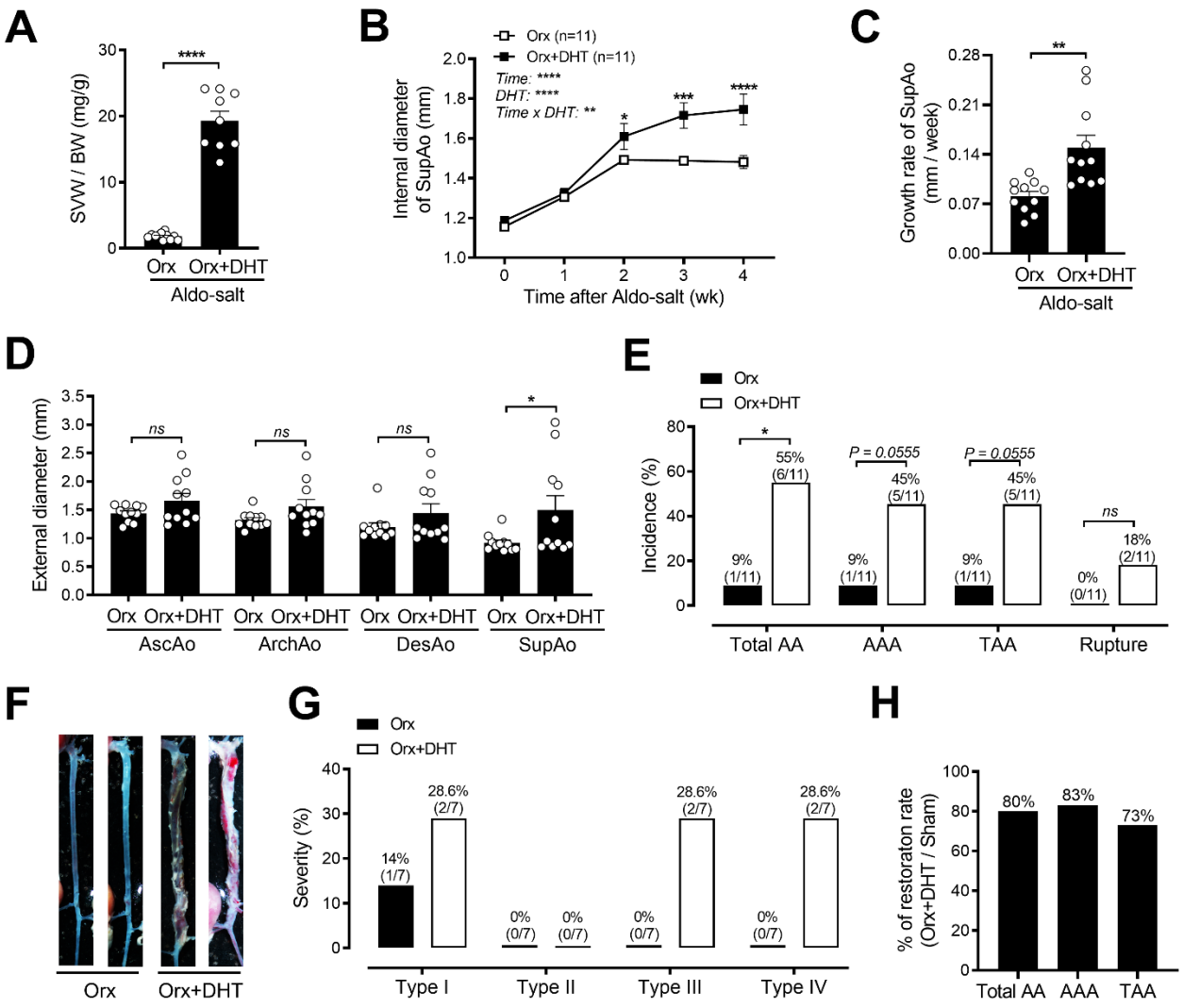

Figure 3. Exogenous dihydrotestosterone administration to orchiectomized male mice restores Aldo-salt-induced aortic aneurysms. (**A**) SVW to BW ratio was determined in 10-month-old orchiectomized (orx) C57BL/6J mice four weeks after Aldo-salt with and without dihydrotestosterone (DHT) pellet implantation (n = 9-11/group). (**B** and **C**) Maximal intraluminal diameters and growth rate of the suprarenal aorta (n = 11/group). (**D**) Maximal external diameters of the AscAo, ArchAo, DesAo, and SupAo (n = 11/group). (**E**) Incidences of total AA, AAA, TAA, and aortic rupture. (**F**) Representative photographs of the aortas with and without aortic aneurysms. (**G**) Severity of aortic aneurysms. (**H**) Restoration rates of aortic aneurysms = mice with orx and DHT and aortic aneurysms / mice with sham-operation and with and without aortic aneurysms. Data were expressed as mean ± SEM and analyzed by two-tailed unpaired *t*-test (**A**, **C**, and **D**), two-way ANOVA with multiple comparison tests (**B**), and two-sided Chi-square test (**E**). **, P <0.05; **, P < 0.01; ***, P < 0.001; ****, P < 0.0001; ns, not significant.*

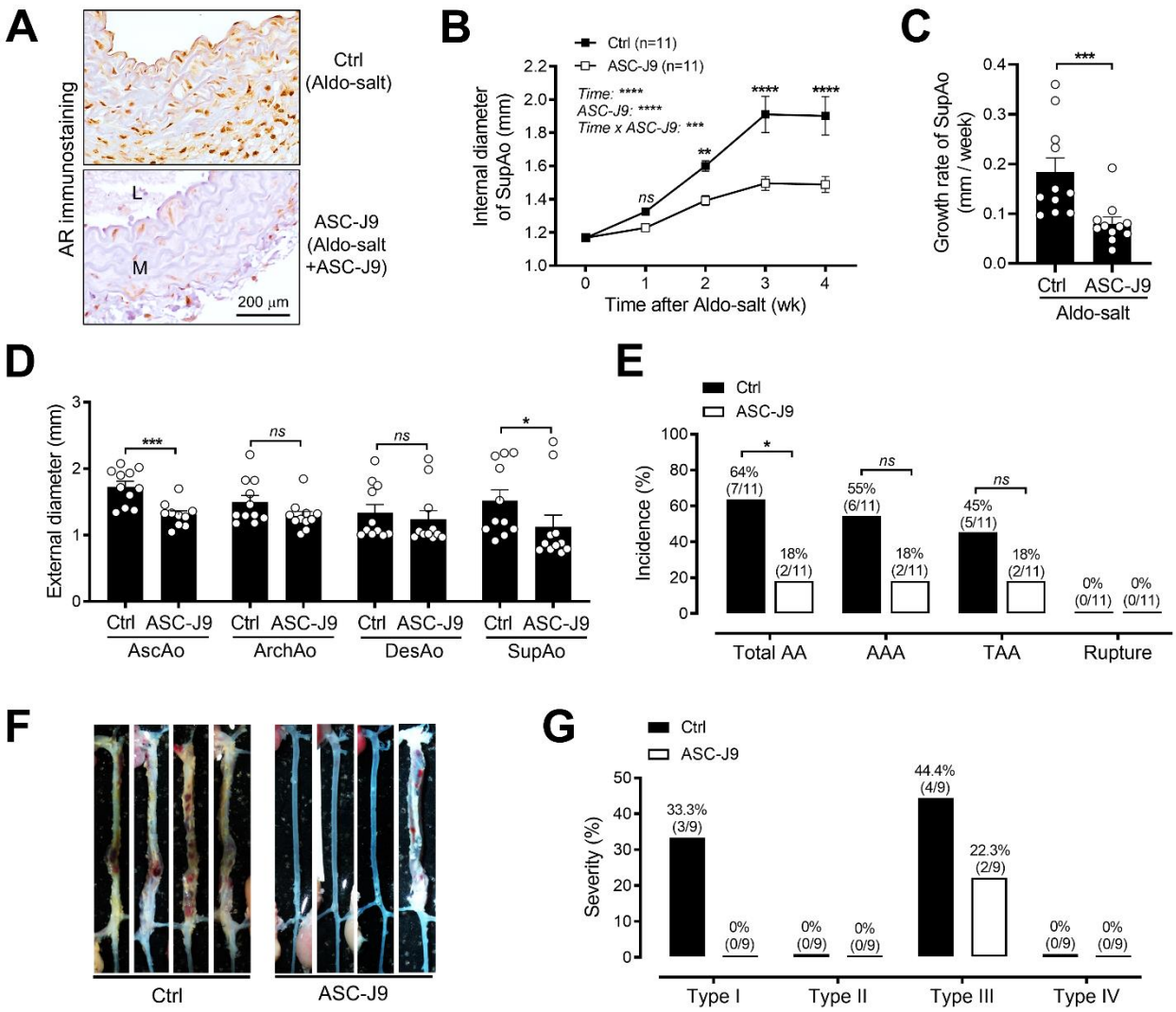

Figure 4. Downregulation of AR by ASC-J9 in mice inhibits Aldo-salt-induced aortic aneurysm. (**A**) Representative immunostaining of AR in the suprarenal aortas from 10-month-old male C57BL/6J mice four weeks after Aldo-salt with and without ASC-J9 administration (n = 3/group). L, lumen. M, media. A, adventitia. (**B** and **C**) Maximal internal diameters and growth rate of the suprarenal aorta (n = 11/group). (**D**) Maximal external diameters of the AscAo, ArchAo, DesAo, and SupAo (n = 11/group). (**E**) Incidences of total AA, AAA, TAA, and aortic rupture. (**F**) Representative photographs of the aortas with and without aortic aneurysms. (**G**) Severity of aortic aneurysms. Data were expressed as mean ± SEM and analyzed by two-way ANOVA with multiple comparison tests (**B**), two-tailed unpaired *t*-test (**C** and **D**), and two-sided Chi-square test (**E**). **, P < 0.05; **, P < 0.01; ***, P < 0.001; ****, P < 0.0001; ns, not significant.*

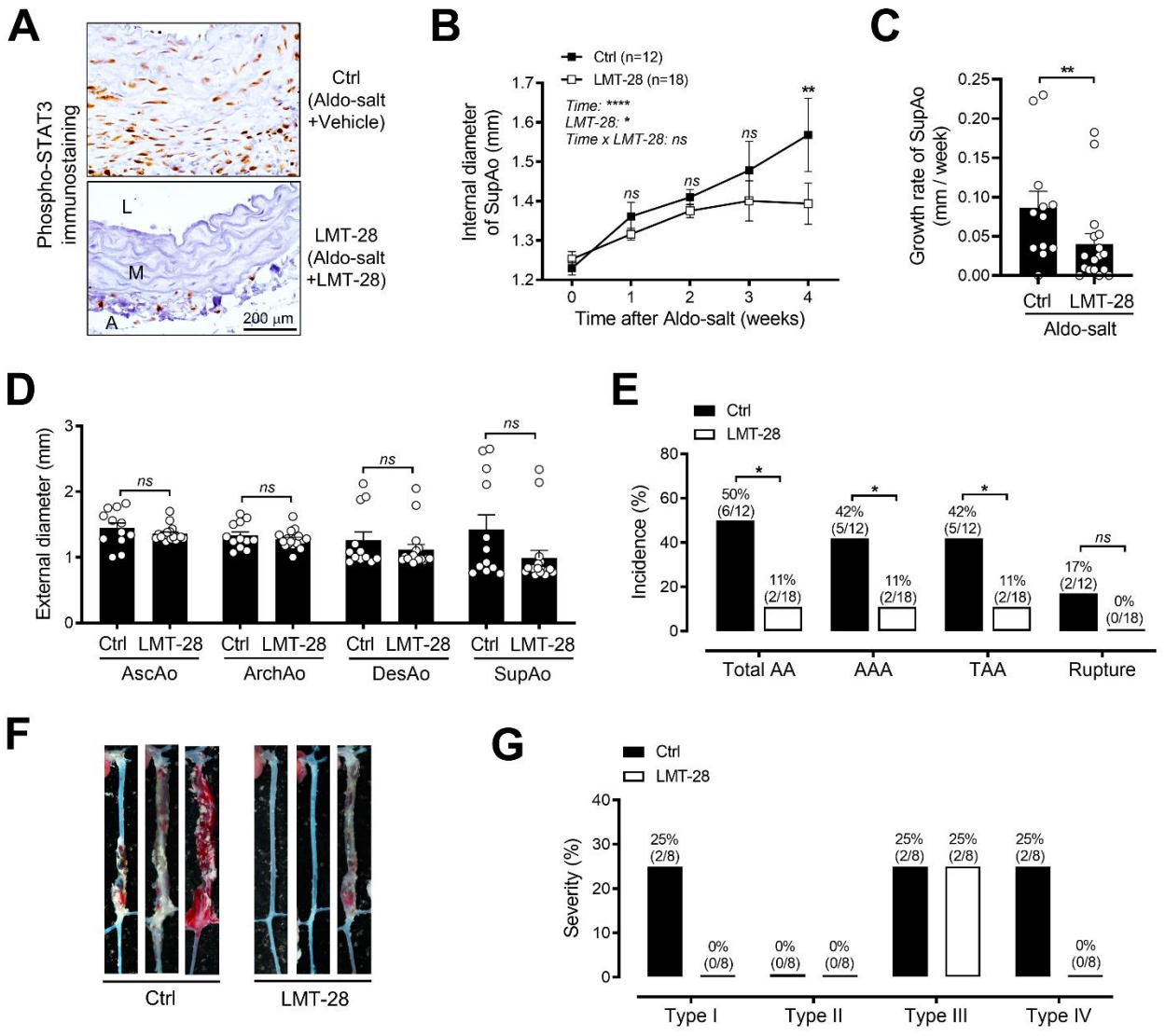

Figure 5. Inhibition of IL-6 signaling by LMT-28 ameliorates Aldo-salt-induced aortic aneurysms. (**A**) Representative immunostaining of STAT3 phosphorylation at Tyr705 in the suprarenal aorta from 10-month-old male C57BL/6J mice four weeks after Aldo-salt with LTM-28 or vehicle controls (Ctrl; n = 3/group). (**B** and **C**) Maximal internal diameters and growth rate of the suprarenal aortas (n = 12-18/group). (**D**) Maximal external diameters of the AscAo, ArchAo, DesAo, and SupAo (n = 12-17/group). (**E**) Incidences of total AA, AAA, TAA, and aortic rupture. (**F**) Representative photographs of the aortas with and without aortic aneurysms. (**G**) Severity of aortic aneurysms. Data were expressed as mean ± SEM and analyzed by two-way ANOVA with multiple comparison tests (**B**), two-tailed unpaired *t*-test (**C** and **D**), and two-sided Chi-square test (**E**). **, p < 0.05; **, p < 0.01; ****, P < 0.0001; ns, not significant.*

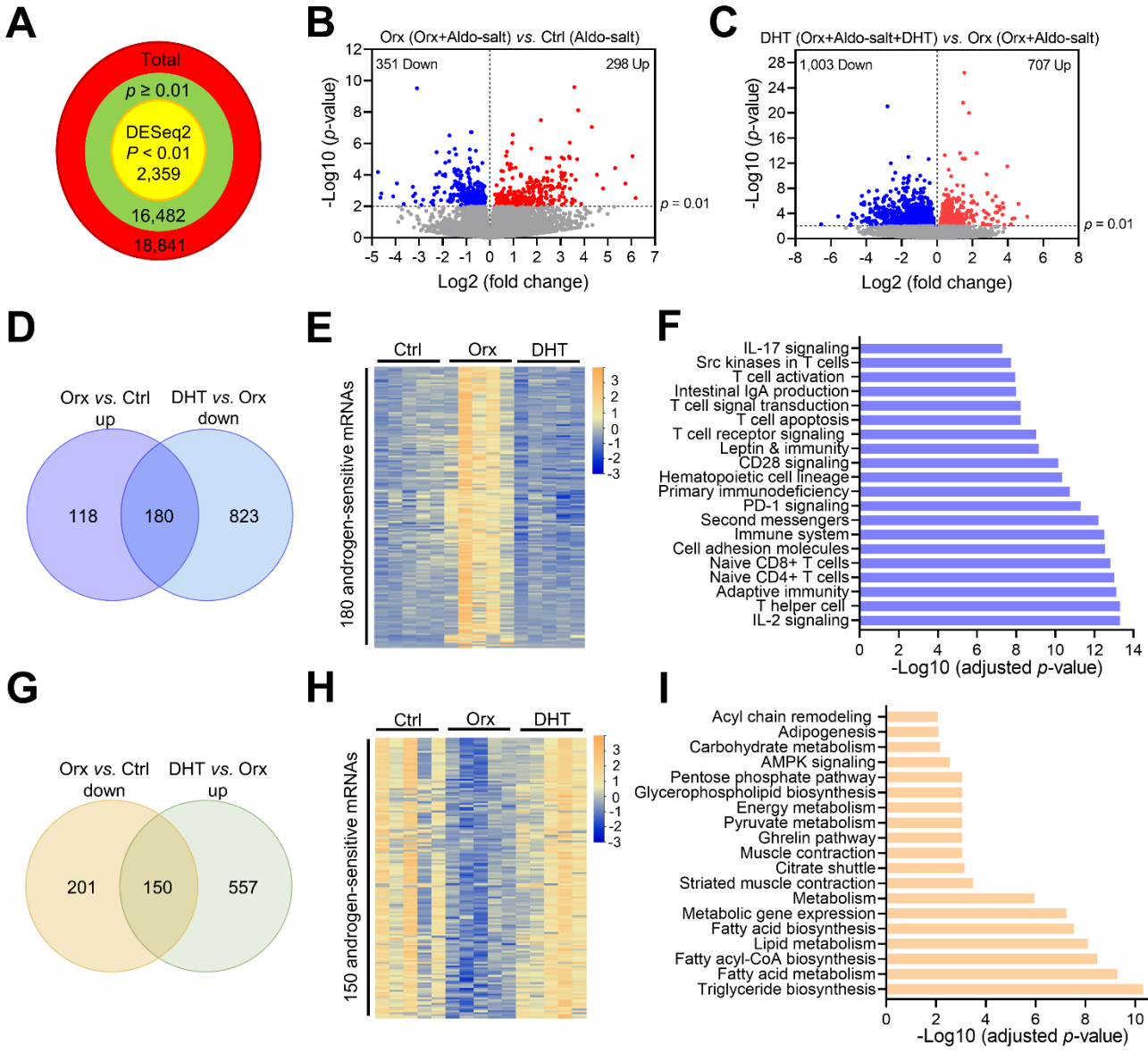

Figure 6. Profiling of aortic transcriptomes reveals T cell receptor signaling as a link between AR and Aldo-salt-induced aortic aneurysms. (**A**) Total numbers of genes whose mRNAs were detected by RNA-seq and analyzed by DESeq2 to be differentially abundant among the whole aortas from 10-month-old C57BL/6J mice with and without orx followed by one-week Aldo-salt with and without DHT pellet implantation (n =5/group). (**B** and **C**) Volcano plot illustration of the number of genes whose mRNAs were analyzed by DESeq2 to be statistically significant (y-axis) *vs.* effect size (fold change, x-axis) in the experiment. (**D** and **G**) Venn diagram identified 180 genes whose mRNAs were upregulated by orchiectomy but downregulated by DHT and 150 genes whose mRNAs were downregulated by orchiectomy but upregulated by DHT, respectively. (**E** and **H**) Heatmap of the 180 genes and 150 genes regulated by androgen (**F** and **I**) Pathway enrichment analysis using Enrichr shows the top 20 pathways among mRNAs that were upregulated by orchiectomy but downregulated by DHT and the 19 pathways among the mRNAs that were downregulated by orchiectomy but upregulated by DHT, respectively.

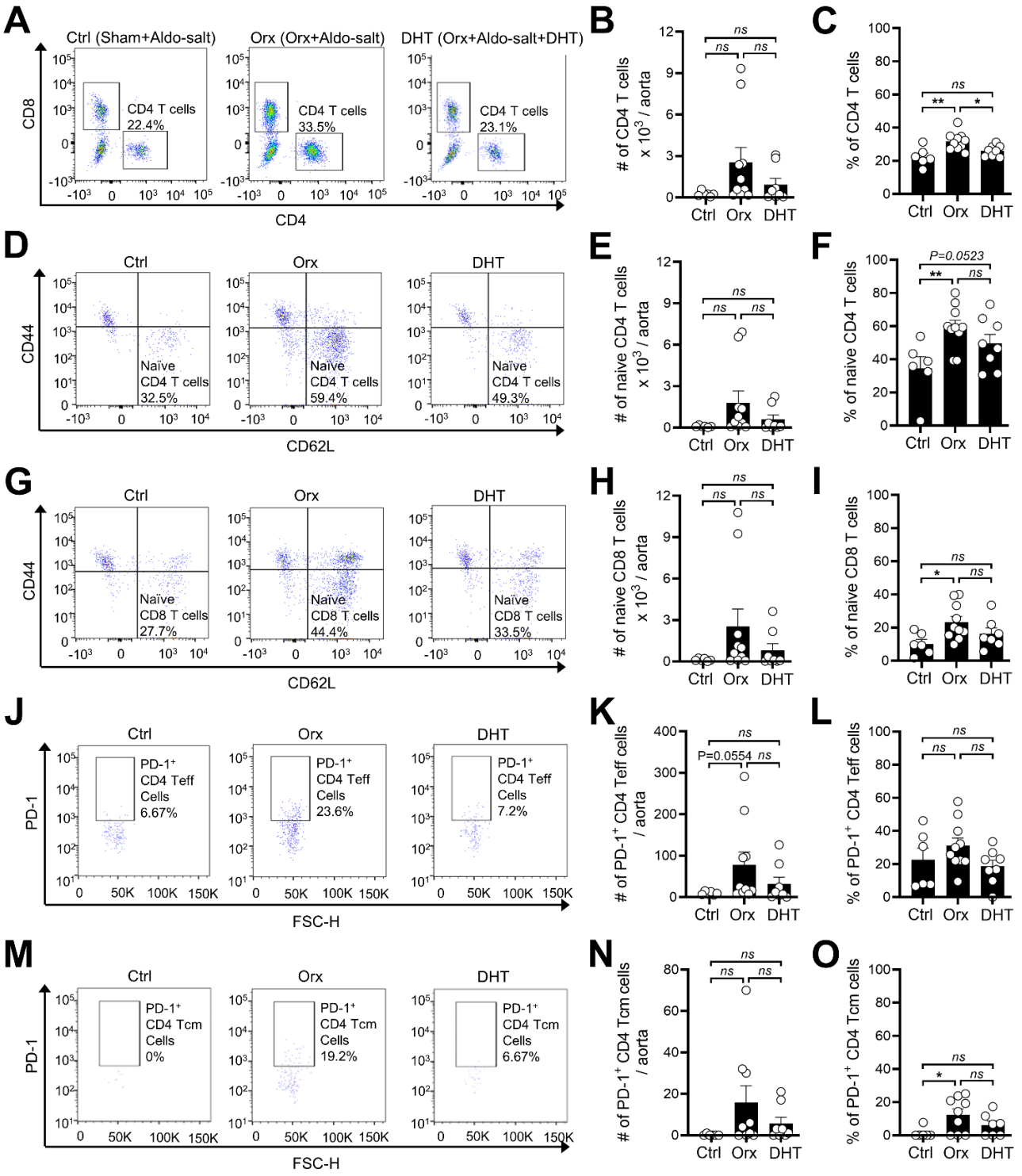

Figure 7. Flow cytometry analysis of T-cell subsets in the aorta in orchiectomized and sham-operated mice ten days after Aldo-salt with and without DHT. Representative pseudocolor plots and quantitative data of the flow cytometry analysis of the total number (#) and percentage (%) of CD4 T-cells ($CD45^+CD3^+CD4^+$; % of total T-cells; **A–C**), naïve CD4 T-cells ($CD45^+CD3^+CD4^+CD44^-CD62L^+$; % of total CD4 T-cells; **D–F**), naïve CD8 T-cells ($CD45^+CD3^+CD8^+CD44^-CD62L^+$; % of total CD8 T-cells; **G–I**), PD-1^+ effector CD4 T-cells (PD-1^+CD4 Teff; $CD45^+CD3^+CD4^+CD44^+CD62L^-CD127^-PD\text{-}1^+$; % of total CD4 Teff cells; **J–L**), and PD-1^+ central memory CD4 T-cells (PD-1^+CD4 Tcm; $CD45^+CD3^+CD4^+CD44^+CD62L^+PD\text{-}1^+$; % of total CD4 Tcm cells; **M–O**) in the whole aorta in 9-10-month-old male C57BL/6J mice with orx or sham operation (Ctrl) ten days after Aldo-salt with and without DHT pellet implantation (n = 6-10/group). The data were expressed as mean ± SEM and analyzed by one-way ANOVA with multiple comparison tests. **, P < 0.05; **, P < 0.01; ns, not significant.*

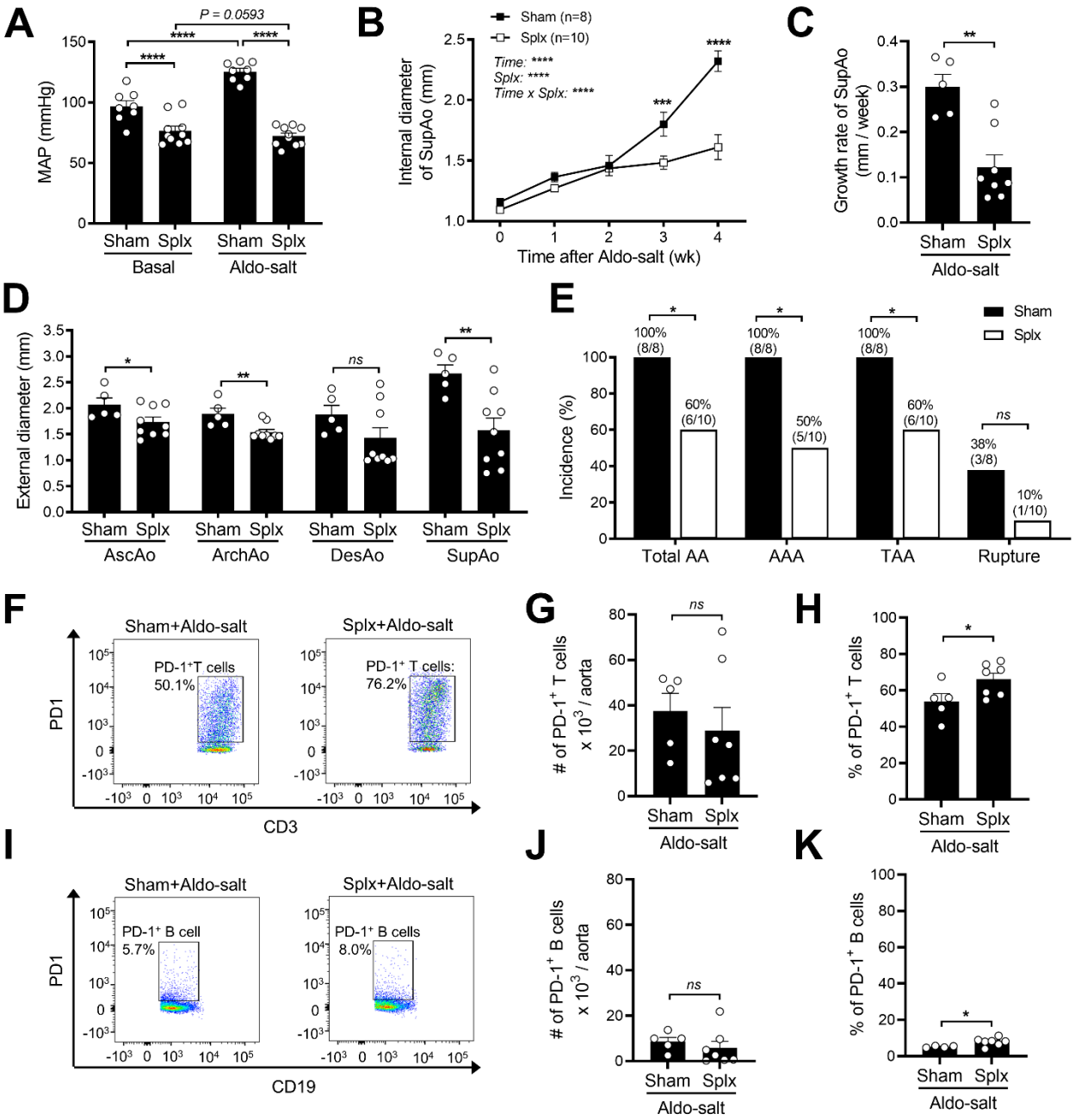

Figure 8. Splenectomy enriches PD-1 positive T- and B-cells in the aorta and mitigates Aldo-salt-induced aortic aneurysms. (**A**) MAP was measured by tail cuff in 11-13-month-old male C57BL/6J mice with splenectomy (splx) or sham operation one week before (basal) and three weeks after Aldo-salt administration (n = 8-10/group). (**B** and **C**) Maximal internal diameters and growth rate of the suprarenal aortas (n = 8-10/group). (**D**) Maximal external diameters of the AscAo, ArchAo, DesAo, and SupAo (n = 5-9/group). (**E**) Incidences of total AA, AAA, TAA, and aortic rupture. (**F**−**K**) Representative pseudocolor plots and quantitative data of the flow cytometry analysis of the total numbers(#) and percentages (%) of PD-1$^+$ T cells (CD45$^+$CD3$^+$PD-1$^+$; % of total T cells) and PD-1$^+$ B cells (CD45$^+$CD19$^+$PD-1$^+$; % of total B cells) in the whole aortas in mice with splx or sham-operation four weeks after Aldo-salt administration (n = 5-7/group). Data were expressed as mean ± SEM and analyzed by two-way ANOVA with multiple comparison tests (**A** and **B**), two-tailed unpaired *t*-test (**C**, **D**, **G**, **H**, **J**, and **K**), and two-sided Chi-square test (**E**). **, P < 0.05; **, P < 0.01; ***, P < 0.001*; *****, P < 0.0001; ns, not significant.*

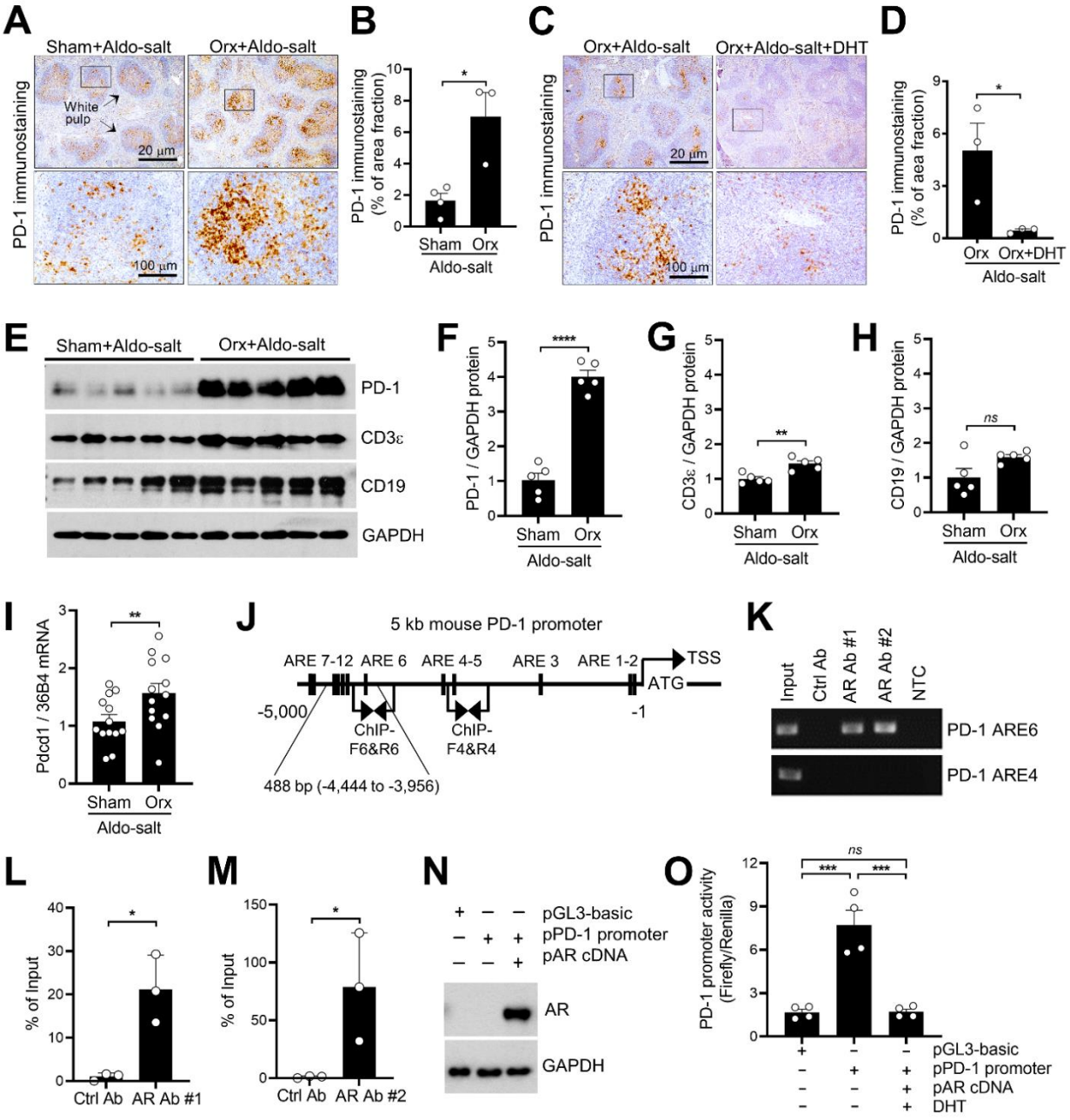

Figure 9. Androgen suppresses PD-1 mRNA and protein expression in the spleen in mice administered Aldo-salt. (**A−D**) Representative immunostainings and quantitative data of PD-1 protein expression in the spleens from 10-month-old male C57BL/6J mice with orx or sham-operation ten days after Aldo-salt administration (n =3-4/group) or orchiectomized mice four weeks after Aldo-salt with and without DHT pellet implantation (n = 3/group). The percentage (%) of areas fraction = (the PD-1 positive area / the area of fields of view) x 100%. The data were calculated from five fields of view randomly photographed per splenic section per mouse. (**E−H**) Representative Western blots and quantitative data of PD-1, CD3ε, CD19, and GAPDH protein expression in the spleens from 10-month-old male mice with orx or sham operation ten days after Aldo-salt administration (n = 5/group). (**I**) Pdcd1 (the gene codes PD-1) mRNA expression in the spleens from 10-month-old male mice with orx or sham operation ten days after Aldo-salt administration (n = 13/group). (**J**) A schematic diagram of the 12 androgen response elements (ARE) in the 5 kb mouse PD-1 promoter. TSS, transcription start site. ATG, translation start codon. ChIP-F, ChIP-PCR forward primers. ChIP-R, ChIP-PCR reverse primers. (**K−M**) Representative and quantitative ChIP-PCR with the control Ab, anti-AR Ab #1, and anti-AR Ab #2 in the spleen (n = 3/group). NTC, no template control. (**N** and **O**) Expression of AR in HEK293 cells suppressed the PD-1 promoter activity (n = 4/group). Data were expressed as mean ± SEM and analyzed by two-tailed unpaired *t*-test (**B**, **D**, **F−H**, **I**, **L**, and **M**) and one-way ANOVA with multiple comparison tests (**O**). **, P < 0.05; **, P < 0.01; ***, P < 0.001*; *****, P < 0.0001; ns, not significant.*

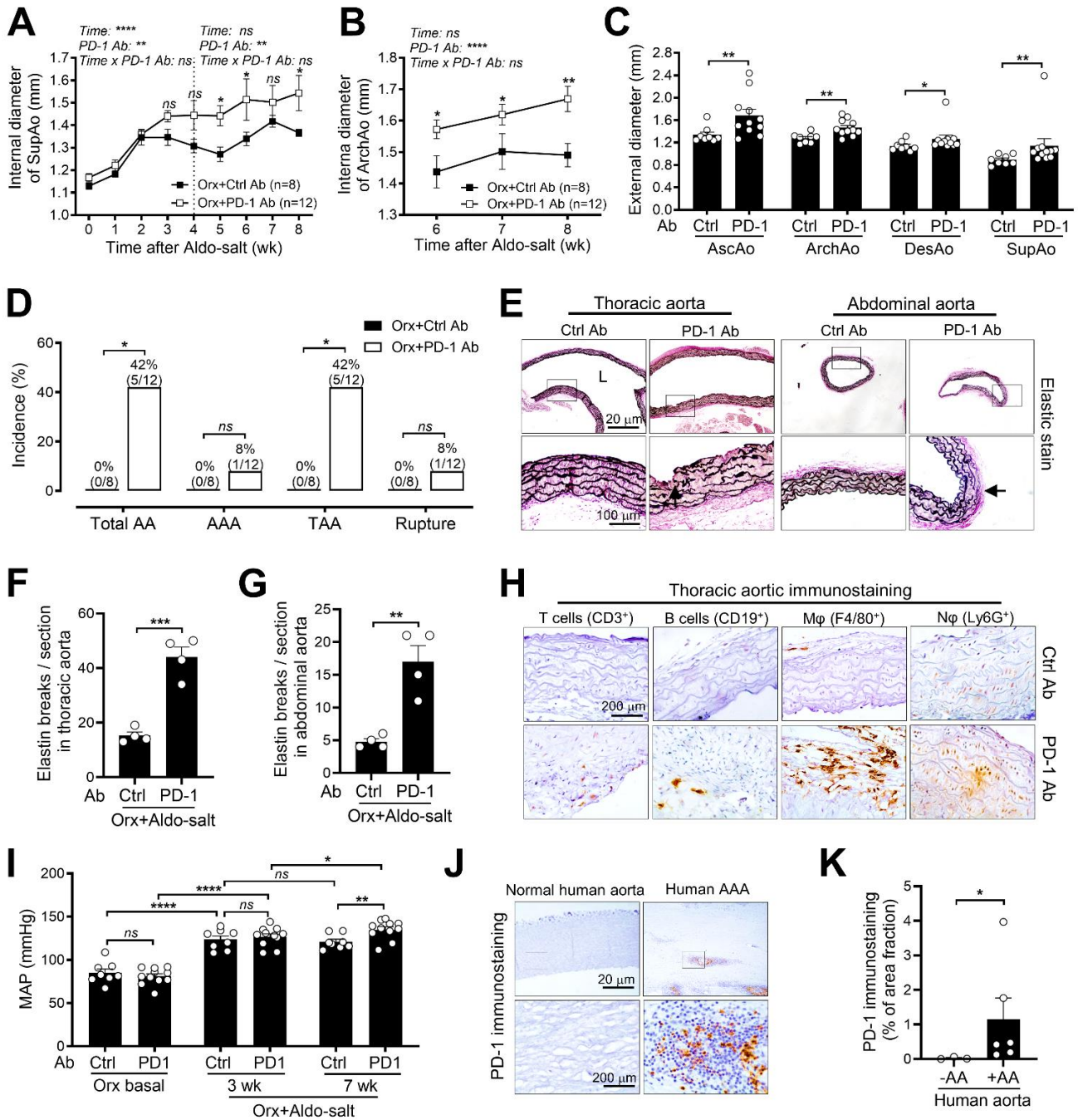

Figure 10. Intraperitoneal injection of anti-PD-1 antibody reinstates Aldo-salt-induced aortopathy in orchiectomized mice. (**A** and **B**) Maximal internal diameters of the suprarenal aorta and aortic arch) in 10-month-old male C57BL/6J mice with orx before and after Aldo-salt with anti-PD-1 or Ctrl Ab injection (n = 8-12/group). (**C**) Maximal external diameters of the AscAo, ArchAo, DesAo, and SupAo (n = 8-11/group). (**D**) Incidences of total AA, AAA, TAA, and aortic rupture. (**E**−**G**) Representative and quantitative Verhoeff-Van Gieson staining of elastin in longitudinal sections of the thoracic aortas and cross-sections of the abdominal aortas in orchiectomized mice with anti-PD-1 or Ctrl Ab eight weeks after Aldo-salt administration (n = 4/group). The arrow indicates elastic breakage. (**H**) Representative immunostaining of T-cells, B-cells, macrophages, and neutrophils in the thoracic aortas in orchiectomized mice eight weeks after Aldo-salt with anti-PD-1 or Ctrl Ab administration (n = 3). (**I**) MAP of orchiectomized mice one week before (basal) and three and seven weeks after Aldo-salt with anti-PD-1 or Ctrl Ab administration (n = 8-11/group). (**J** and **K**) Representative immunostainings and quantitative data of PD-1 protein expression in the human aortas with and without aortic aneurysms (n = 3-6/group). Data were expressed as mean ± SEM and analyzed by two-way ANOVA with multiple comparison tests (**A**, **B**, and **I**), two-tailed unpaired *t*-test (**C**, **F**, **G**, and **K**), and two-sided Chi-square test (**D**). **, P < 0.05; **, P < 0.01; ***, P < 0.001; ****, P < 0.0001 ;ns, not significant.*

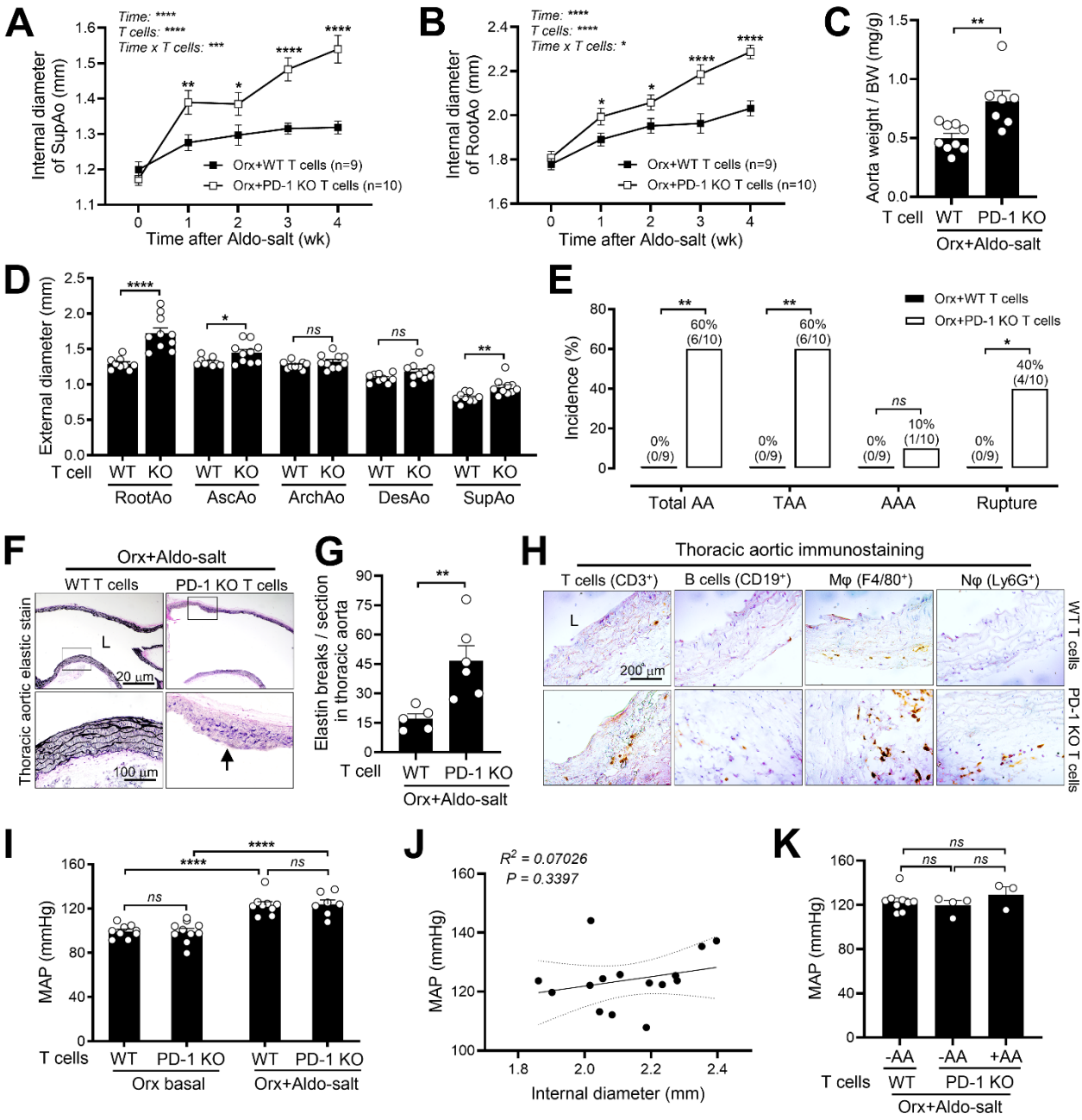

Figure 11. Adoptive PD-1 deficient T cell transfer restores Aldo-salt-induced aortopathy in orchiectomized mice. (**A** and **B**) Maximal internal diameters of the suprarenal aorta and aortic root in 9-10-month-old orchiectomized male C57BL/6J mice with adoptive PD-1-KO and WT T-cell transfer via retro-orbital sinus injection two days before and eight and eighteen days after Aldo-salt administration (n = 9-10/group). PD-1 KO and WT T cells were isolated from the spleens of 4-month-old male PD-1 KO and WT C57BL6J mice via anti-CD90.2 magnetic beads. (**C**) Aortic weight to BW ratio (n = 7-9/group). (**D**) Maximal external diameters of the RootAo, AscAo, ArchAo, DesAo, and SupAo (n = 9-10/group). (**E**) Incidences of total AA, AAA, TAA, and aortic rupture. (**F** and **G**) Representative and quantitative elastin stain in the longitudinal sections of the thoracic aortas (n = 5-6/group). The arrow indicates elastic breakage. (**H**) Representative immunostaining of T-cells, B-cells, macrophages (Mφ), and neutrophils (Nφ) in the thoracic aortas (n = 3). (**I**) MAP was measured by tail cuff one week before (basal) and three weeks after Aldo-salt administration (n = 8-10/group). (**J**) Correlation analysis of the internal diameter of the aortic root and MAP three weeks after Aldo-salt administration (n = 15/group). (**K**) MAP in mice with (+) and without (-) Aldo-salt-induced aortic aneurysms (n = 3-9/group). Data were expressed as mean ± SEM and analyzed by two-way ANOVA with multiple comparison tests (**A**, **B**, and **I**), two-tailed unpaired *t*-test (**C**, **D**, and **G**), two-sided Chi-square test (**E**), simple linear regression analysis (**J**), and one-way ANOVA for multiple comparison tests (**K**). *, *p<0.05; **, p<0.01; ***, p<0.001; ****, p<0.0001; ns, not significant.*

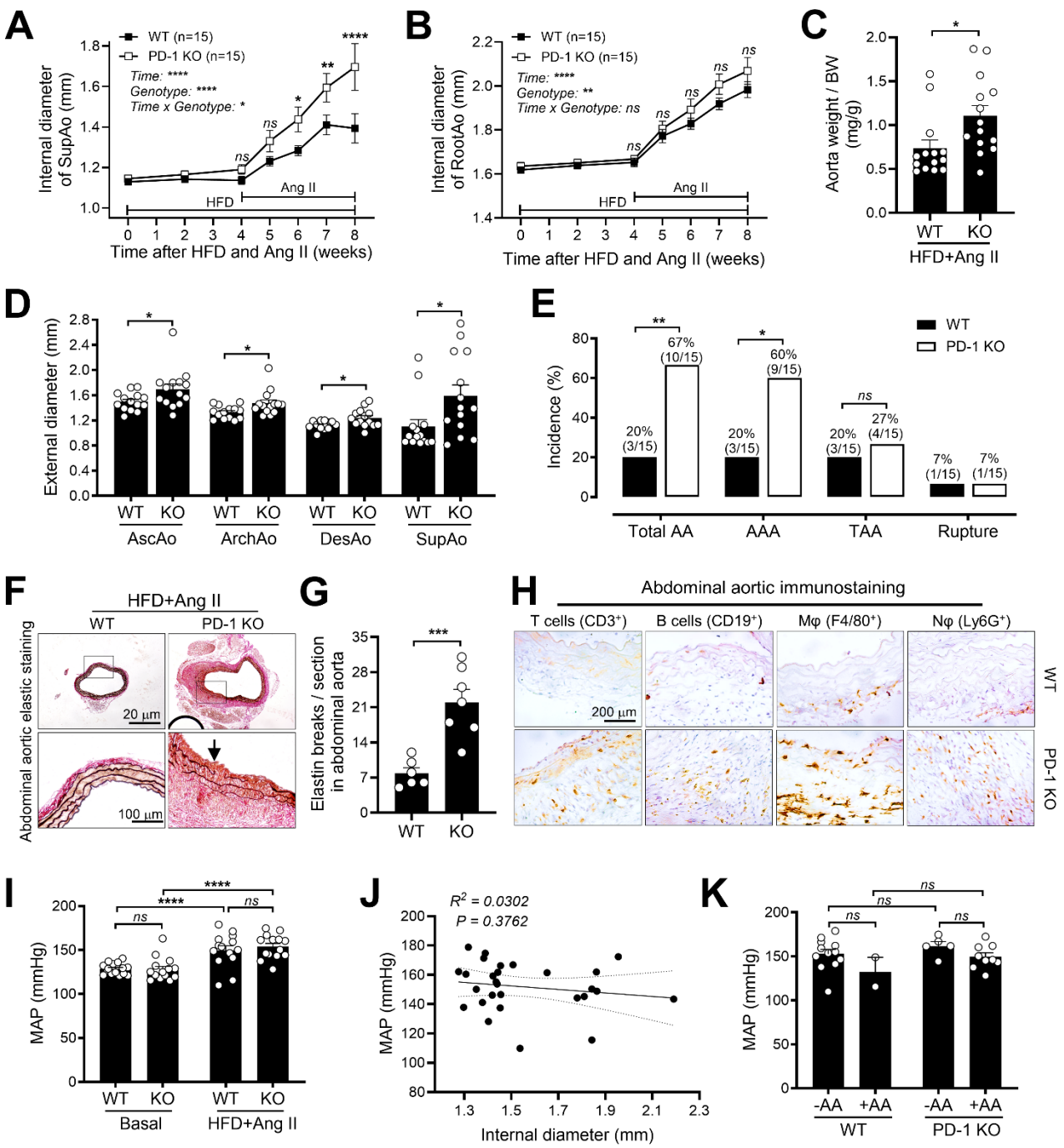

Figure 12. Genetic deletion of PD-1 exacerbates high-fat diet and angiotensin II-induced aortopathy. (**A** and **B**) Maximal internal diameters of the suprarenal aorta and aortic root in 2-month-old male PD-1-KO and WT C57BL/6J mice with eight-week high-fat diet (HFD) feeding and four-week Ang II infusion (n = 15/group). (**C**) Aortic weight to BW ratio (n = 14/group). (**D**) Maximal external diameters of the AscAo, ArchAo, DesAo, and SupAo (n = 14/group). (**E**) Incidences of total AA, AAA, TAA, and aortic rupture. (**F** and **G**) Representative and quantitative Verhoeff-Van Gieson elastin staining in the abdominal aortas. The arrow indicates elastic breakage (n = 6-7/group). (**H**) Representative immunostaining of T-cells, B-cells, macrophages, and neutrophils in the abdominal aortas (n = 3). (**I**) MAP was measured by tail cuff one week before (basal) and three weeks after HFD and Ang II administration (n =14-15/group). (**J**) Correlation analysis of the internal diameter of the suprarenal aorta and MAP in PD-1 KO and WT mice three weeks after HFD and Ang II administration (n = 28/group). (**K**) MAP with (+) and without (-) aortic aneurysms (n =2-12/group). Data were expressed as mean ± SEM and analyzed by two-way ANOVA with multiple comparison tests (**A**, **B**, **I**, and **K**), two-tailed unpaired *t*-test (**C**, **D**, and **G**), two-sided Chi-square test (**E**), and simple linear regression analysis (**J**). **, P < 0.05; **, P < 0.01; ***, P < 0.001; ****, P < 0.0001; ns, not significant.*